SINGLE LAYERS OF THE METALLIC LAYERED COMPOUNDS TaS_2 AND NbS_2

by

Liu, Chian

B.Sc. Wuhan University, 1969

A THESIS SUBMITTED IN PARTIAL FULFILLMENT OF
THE REQUIREMENTS FOR THE DEGREE OF
MASTER OF SCIENCE
in the Department
of
Physics

SIMON FRASER UNIVERSITY
July 1982

APPROVAL

Name: Liu, Chian

Degree: Master of Science

Title of Thesis: Single Layers of the Metallic Layered Compounds TaS_2 and NbS_2

Examining Committee:

Chairman: B.P. Clayman

R.F. Frindt
Senior Supervisor

A.E. Curzon

E.D. Crozier

S.R. Morrison
External Examiner
Professor
Department of Physics
Simon Fraser University

Date Approved: 30 July /82

Title of Thesis/Project/Extended Essay

Single Layers of the Metallic Layered Compounds TaS_2 and NbS_2

Author:

(signature)

Liu, Chian

(name)

30 July, 1982

(date)

ABSTRACT

Freely floating single layers of the metallic layered compounds TaS_2 and NbS_2 up to 2000Å in lateral size were obtained by the intercalation of hydrogen and water into single crystals of 2H-TaS_2 and 2H-NbS_2 followed by ultrasonic dispersion. Prior to dispersion, the single layers were investigated by X-ray diffraction. It was found that each layer was separated by at least 100Å of intercalated water. On deintercalation of water the layers tend to stack back to the original structure. The single layers retain the same structure as the original host crystal with the a parameter remaining unchanged to within one percent. Crystals that are restacked from single layer dispersions appear to have a random layer stacking sequence.

Optical absorption studies were carried out for single layer dispersions of TaS_2 and NbS_2. The absorption spectra of single layer suspensions or in the randomly stacked form are similar to those of 2H-TaS_2 and 2H-NbS_2 single crystals for $\vec{E} \perp \vec{c}$.

A magnetic field was used to align the single layers in suspension, and optical absorption measurements were carried out on single layer NbS_2 in the range 1.77 to 3.1 eV for $\vec{E} \parallel \vec{c}$ and $\vec{E} \perp \vec{c}$. The interband transition observed at 2.7 eV for $\vec{E} \perp \vec{c}$ was observed to be almost completely suppressed for $\vec{E} \parallel \vec{c}$. This observation is compared to optical anisotropy measurements by other workers on crystals of 2H-$NbSe_2$ and 3R-NbS_2 and supports the generally held view that the 3R structure is more "two-dimensional" than the 2H structure. The optical observations on single layers are also discussed in terms of energy band models for the metallic layered compounds and will be useful in band structure transition assignments for the optical features observed in these compounds.

Studies on suspensions of small crystallites (not necessarily single layers) of the layered compounds aligned in a magnetic field should be a new and useful technique for studying the optical anisotropy of layered compounds.

ACKNOWLEDGEMENTS

I wish to express my sincere thanks to my supervisor, Professor R.F.Frindt, for his constant encouragement, concrete guidance and helpful discussions throughout this research and for his kindness in correcting the hand written manuscript of my thesis which occupied a great deal of his time.

Thanks also to Professors A.S.Arrott, M.Plischke, A.E. Curzon, E.D.Crozier, S.Gygax and L.E.Ballentine for the helpful discussions with them; to Per Joenson for the technical help, in particular for preparing 2H-NbS_2 single crystals for me; to Dr. O.Singh for taking the electron microscope photographs; to Dr. G.A.Scholz for many friendly talks and helpful discusions; and to Marion Jaques for typing part of this thesis.

Finally, the help from the technical and secretarial staff of the Physics Department is also very appreciated.

A scholarship from the Chinese Government and the partial financial support provided by my supervisor and the Natural Sciences and Engineering Council of Canada are also very gratefully acknowledged.

TABLE OF CONTENTS

LIST OF TABLES

LIST OF FIGURES

Chapter 1

Introduction

For a long time there has been a wide interest in two-dimensional systems both in theoretical and experimental fields of research in physics. In the words of Professor J.G. Dash (1982), "the study of two-dimensional matter would seem to be a completely theoretical branch of physics, were it not that such matter actually exists". Various two-dimensional systems, such as two-dimensional gases, liquids and crystalline solids, mono-molecular films adhering on the surfaces of solids, two-dimensional random lattices, etc., have been proposed and their structure and properties are of considerable current interest.

The transition metal dichalcogenides, well-known for their layer and pseudo two-dimensional structure and various fascinating properties, have been the subject of world-wide study in the fields of both physics and chemistry since about 1960. This work includes studies of electrical and optical anisotropy, charge density wave formation, superconductivity of the pure and organically intercalated crystals, Raman studies, metallic intercalation and order-disorder transition of metallic intercalates. To what extent the pure materials and also the intercalated systems are "two-dimensional" or approximate a single layer continues to be a subject of

discussion and debate in almost all the papers on layered systems. Studies on single layers will be able to help clarify this question and it is felt that this thesis is the start of such studies. The thesis is basically concerned with the preparation of single layers of the metallic layered compounds TaS_2 and NbS_2, X-ray studies of such layers and a study of the anisotropy in optical absorption of suspensions of single layers aligned in a magnetic field. The magnetic field alignment technique is novel and is not restricted to single layers. It could be applied in various anisotropic studies on many other layered compounds.

1.1 Structure and Properties of 2H-TaS_2 and 2H-NbS_2

1.1.1 Structure

2H-TaS_2 and 2H-NbS_2 belong to the family of layered transition metal (from groups IVB, VB and VIB) dichalcogenides. As summarized in an early review paper by Wilson and Yoffe (1969), layered transition metal dichalcogenides have a structure made up from "molecular sandwiches", each sandwich made up of a sheet of transition metal atoms in between two sheets of chalcogen atoms. The atoms in a sandwich are hexagonally packed (not close packed) through strong and primarily covalent bonds, while the sandwiches are held together by weak van der Waals forces. This structure is

represented by the familiar sectional scheme as shown in Fig. 1.1.

The sandwich containing three sheets of hexagonally packed atoms is called a molecular layer. For this reason the names of "layer material" and "layer compounds" are also used for layered transition metal dichalcogenides. Depending on the stacking sequence of the layers, there are several polytypes in layered materials, especially in the group VB materials. Most of the members of the other groups fall into just one co-ordination class. So far as we know, TaS_2 has four polytypes labelled 1T, 2H, 4Hb and 6R, while NbS_2 has only 2H and 3R polytypes (Fisher and Sienko, 1980). In this abbreviated notation, the integer indicates the number of layers per unit cell along the hexagonal symmetry axis (c or z), and T, H and R denote the trigonal, hexagonal and rhombohedral primitive unit cells respectively. In the 1T polytype of TaS_2, for example, the Ta atom is octahedrally coordinated by sulphur atoms while in the 2H phase the co-ordination is trigonal prismatic (Fig. 1.2). In the 4Hb and 6R polytpes, the coordination within successive layers alternates between octahedral and trigonal prismatic (see Mattheiss, 1973).

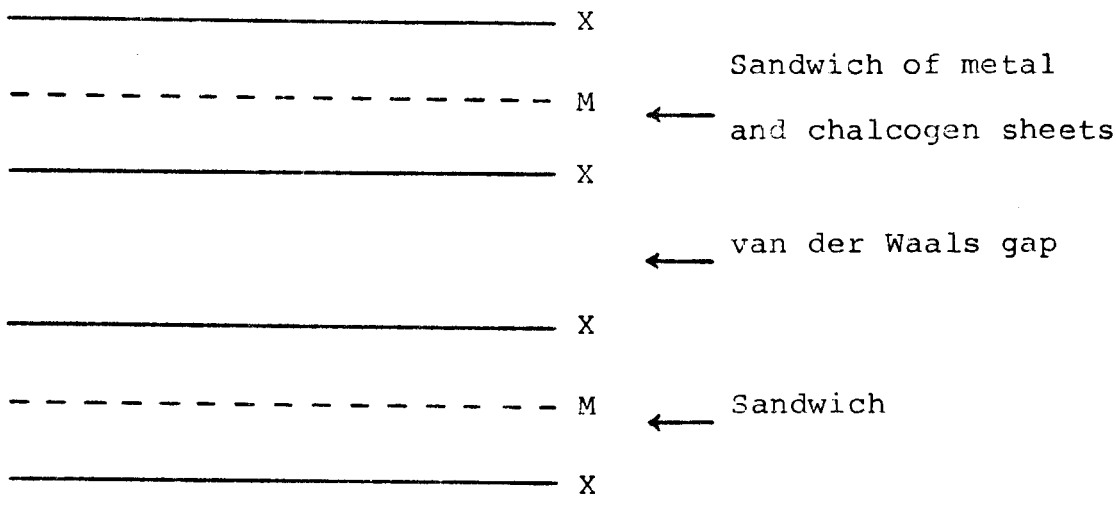

X: Chalcogen atoms

M: Transition metal atoms.

Fig.1.1: General form of layered transition metal dichalcogenide structure (in section).

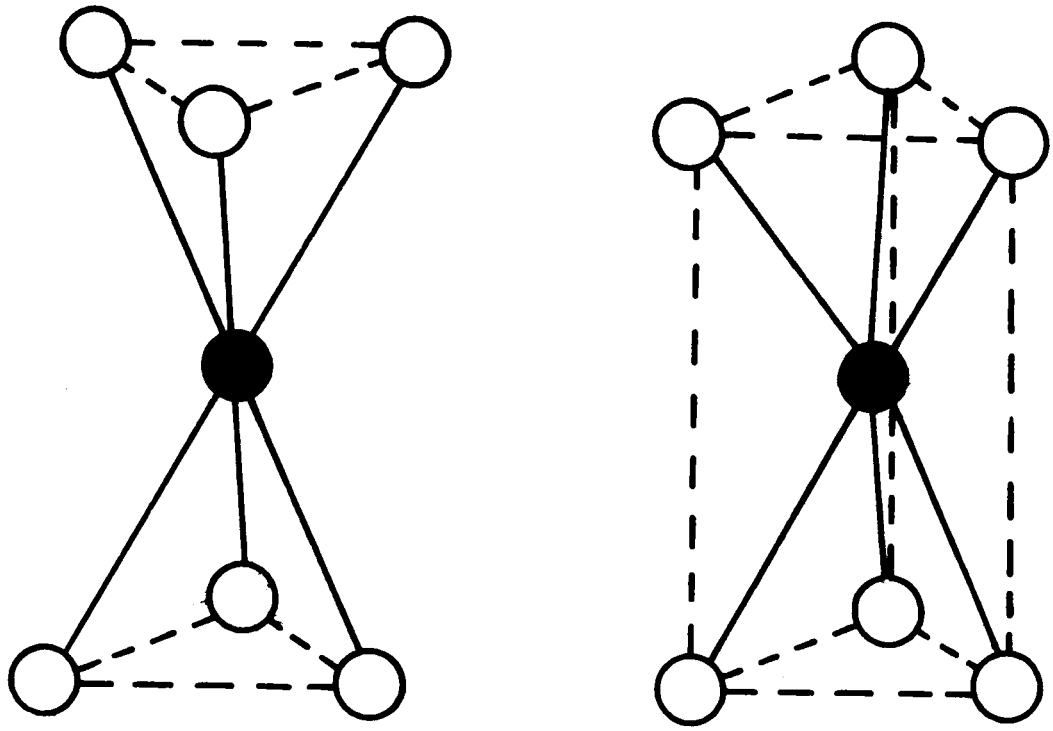

(a) Octahedron

(b) Trigonal Prism

Fig. 1.2: Octahedral and trigonal prismatic coordinations.

2H-TaS_2 and 2H-NbS_2 have the same structure and belong to the D_{6h}^4 ($P6_3/mmc$) space group, where $P6_3/mmc$ is the Hermann-Mauguin symbol adopted in the International Tables for X-ray crystallography (1952). $P6_3/mmc$ means a primitive cell in which a sixfold screw axis with translation 3/6 is normal to a mirror plane and parallel to another mirror plane and a c glide plane. D_{6h}^4 is Schoenflies' notation describing the same space group (Phillips, 1963). The structure and unit cell of 2H-TaS_2 and 2H-NbS_2 are shown in Fig. 1.3, where the metal atom is trigonal prismatically coordinated by sulphur atoms. The structure parameters are a = 3.315Å and c= 2 × 6.05Å for 2H-TaS_2 (Jellinek, 1962) and a = 3.31Å and c = 2 × 5.945Å for 2H-NbS_2 (Jellinek et al, 1960). The separation of the neighbouring tantalum (niobium) and sulphur planes is approximately equal to 1/8 c (Mattheiss, 1973) and following Slater (1965) and Mattheiss (1973), if we choose a new coordinate system o'x'y'z' (Fig. 1.3), the fractional unit cell atomic coordinates can be written as (0,0,1/4) for the metal atoms and (1/3, 2/3, 1/8) and (1/3, 2/3, 3/8) for the sulphur atoms.

1.1.2 General Properties of Layer Compounds

A total of about 60 layer compounds make up the transition metal dichalcogenides. A very wide range of properties are exhibited by the compounds. Electrically, most

Fig.1.3: (a) Atomic structure of 2H-TaS_2 and 2H-NbS_2
(b) Conventional unit cell ($11\bar{2}0$ section) of 2H-TaS_2 and 2H-NbS_2.

● Tantalum or Niobium Atom

○ Sulfur Atom.

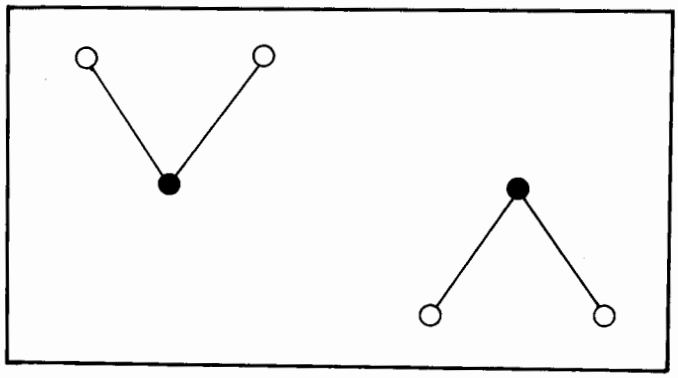

(b)

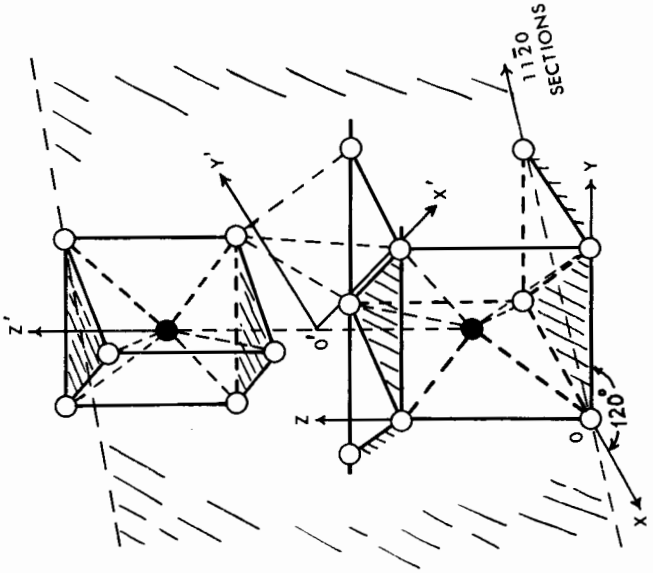

(a)

of the group IVB and VIB compounds are semiconductors (some of them are semimetals and insulators), while group VB compounds are mostly metals. Furthermore, most of the Nb and Ta compounds are superconductors. Due to the weak interlayer coupling, the anisotropy in electric conductivity of all the layer compounds is extremely large. For example, for the metallic compounds, the room temperature conductivity perpendicular to the layers is typically 30 to 50 times smaller than that parallel to the layers.

The weak interlayer coupling allows a wide range of metals and other electron donors such as ammonia and pyridine to be intercalated into the van der Waals' gap between the layers. The intercalation causes an increase in the interlayer separation, by as much as 50Å in some cases, but does not appear to change the structure type of the host material. A small increase in the host a axis parameters is also generally observed. The host material tends to revert back to its original structure after deintercalation.

The strong intralayer bonding and the very weak interlayer coupling makes the layer compounds very anisotropic mechanically. As a result, it is not difficult to get, by repeated cleaving of a layer material, a thin crystal a few hundred angstroms thick. Such thicknesses are ideal for optical transmission studies in band gap and interband absorption regions where the absorption constant attains

values of 10^5 to $10^6 cm^{-1}$. By contrast, such studies of other non-layer metals and semiconductors are hampered by the difficulty of making very thin samples. Although thin films can be made on transparent substrates using vacuum evaporation, sputtering or chemical deposition techniques, thin films made by these methods are often different in structure from the bulk material. Because suitable transmission samples are readily made, and also because most layered crystals can be prepared with specular surfaces ideal for reflection studies, the optical constants of most layer compounds have been extensively investigated. Various theoretical calculations of the energy band structures of these materials have also been carried out and compared with the experimental results. In most cases, the measured optical transmission and reflection spectra can be interpreted in terms of specific excitonic or interband transitions from the calculated band structures.

The general features of the band structures of these layer compounds are representd by a predominantly p-like valence band and a mainly s-like conduction band with a manifold of d-character bands in between. A schematic diagram of these band structures is shown in Fig. 1.4 (Yoffe, 1974). The energy gap between valence and conduction bands is usually several electron volts. The transmission spectra of group VI semiconducting compounds are characterized by a pair of

Fig.1.4: Schematic diagram of simple model band structures of
(a) Group VI compounds (MoS_2)
(b) Group V compounds (NbS_2, TaS_2)
(c) Group IV compounds (ZrS_2)
(followed Yoffe (1974)).

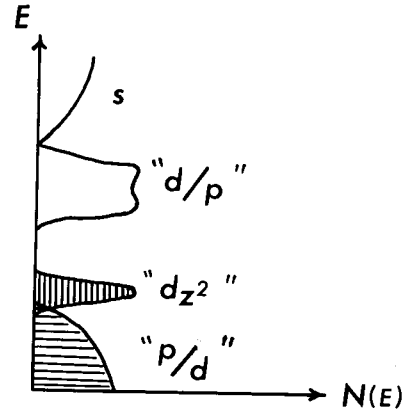

(a) VI

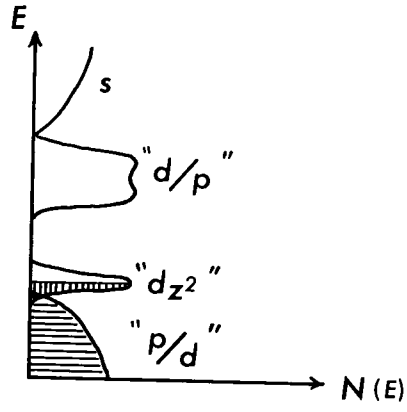

(b) V

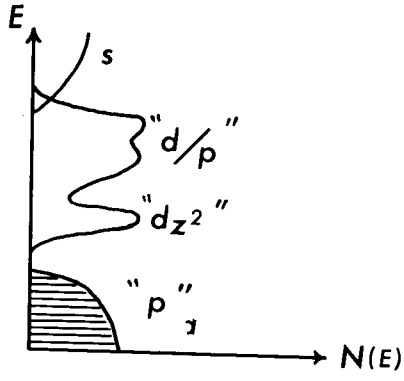

(c) IV

exciton peaks which are interpreted as resulting from a spin-orbit split valence band. For the group V metallic compounds, these exciton peaks are screened out by the free carriers. A large number of free carriers exist in the group V compounds due to the fact that the so-called d_{z2} band (Fig. 1.4) is only half full. These free carriers are responsible for rise in absorption below about 1 eV. For the group VI compounds, the d_{z2} band is full and the semiconducting behaviour results. There is a strong, broad absorption in the region of a few eV for all the group IV, V and VI layer compounds. This corresponds to the interband transitions from valence bands to empty conduction bands.

Many original optical spectra of both metallic and semiconducting layer compounds can be found in Wilson and Yoffe's article (1969). More recent work on the group V metallic compounds is found in the paper by Beal et al (1976).

1.1.3 Properties of Metallic 2H-TaS_2 and 2H-NbS_2

The metallic compounds 2H-TaS_2 and 2H-NbS_2 have very similar properties. Single crystals of 2H-TaS_2 and 2H-NbS_2 have a greyish metallic appearance with wrinkled surfaces. They are usually grown from the synthesized charge by means of

iodine vapor transport (Schafer, 1962; Brixner, 1962). Typically they have a size of 0.1 to 0.01 mm thick and 10 mm^2 to 1 cm^2 in area. The mass density of 2H-TaS_2 is about 7.02 g/cm^3 and for 2H-NbS_2 is 4.62 g/cm^3 as we calculated from the molecular mass and lattice parameters. The electrical resistivities of 2H-TaS_2 at room temperature are 150 (±10%)$\mu\Omega\cdot cm$ parallel to the layers and 4900 (±25%) $\mu\Omega\cdot cm$ perpendicular to the layers (Tidman et al, 1974; Thompson et al, 1972).

The transmission spectra of metallic 2H-TaS_2 and 2H-NbS_2 (Fig. 1.5) are characterized by broad absorption peaks at about 3 eV, with a steep drop and a local absorption minimum around 1.2 to 1.4 eV (Wilson and Yoffe, 1969; Beal and Liang, 1973). This rise in absorption is due to free carrier absorption.

A schematic one-electron energy band diagram of 2H-TaS_2 and 2H-NbS_2 is shown in Fig. 1.4 and compared with that of MoS_2 and ZrS_2. The half-filled d_{z2} band determines the metallic properties and the high free carrier absorption in 2H-TaS_2 and 2H-NbS_2.

2H-TaS_2 becomes superconducting at temperatures below 0.8°K while for 2H-NbS_2 the superconducting transition temperature T_c is around 6.3°K (Maaren and Schaefer, 1966; Gamble et al, 1971b). It is noted that the intercalation of organic molecules has a great influence on T_c. For 2H-NbS_2

Fig.1.5: Optical absorption spectra of
(a) 2H-TaS_2 (Beal and Liang, (1973)) and
(b) 2H-NbS_2 (Wilson and Yoffe, (1969))
at 77 K.

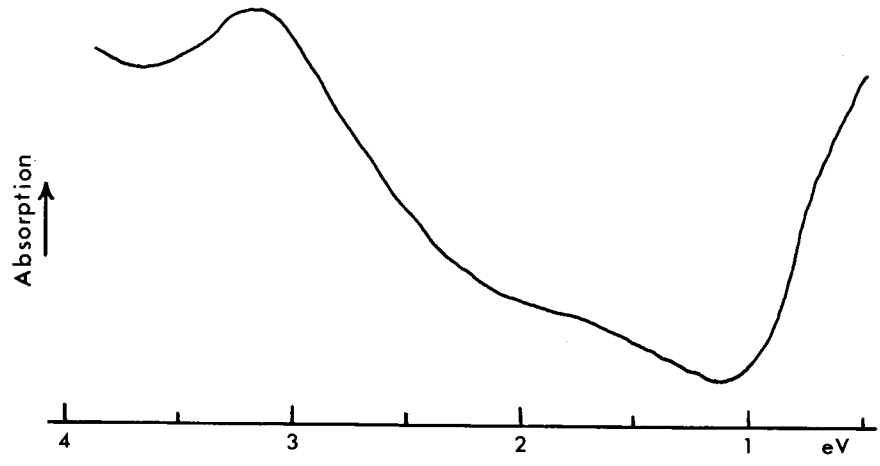

(a)

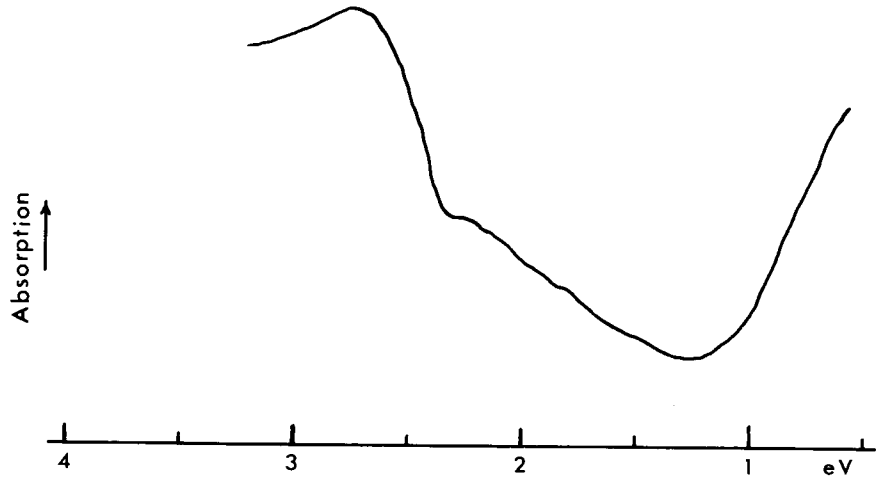

(b)

T_c is always lower after intercalation, while for 2H-TaS_2 T_c is increased after intercalation (Gamble et al, 1970, 1971a).

A remarkable property of both 2H-TaS_2 and 2H-NbS_2 is that they can be more easily intercalated by a large range of guest species. Of particular interest to the work presented in this thesis is that a large expansion along the c axis can be obtained by the electrointercalation of hydrogen ions and water molecules (Murphy and Hull, 1975; Whittingham, 1974). This makes it possible to obtain a suspension of freely floating single molecular layers of both TaS_2 and NbS_2 in water.

This thesis identifies the single layer form of TaS_2 and NbS_2 by using Debye-Scherrer X-ray powder photography. Such X-ray patterns have not been previously published. Other evidence confirming the single layer form of these crystals is also presented.

The method used to make single layer TaS_2 and NbS_2 suspension in water is similar to that developed by Murphy and Hull (1975). But the present method is much simpler and more easily carried out. Attempts to make single layers using 2H-$NbSe_2$, 2H-MoS_2 and 1T-TaS_2 have been unsuccessful.

The optical transmission of single layer NbS_2 suspension in water has been investigated by using a double beam technique in the wavelength range from 4000 to 7000Å. A Cary 17 double

beam spectrometer was also used in the region from 3000 to 14000Å for comparison.

It was interestingly observed that the single layers of TaS_2 and NbS_2 in water aligned up in a magnetic field greater than several kilogauss in the direction perpendicular to the field. Using polarized light the optical absorption properties of NbS_2 both in $\vec{E} \perp \vec{c}$ and $\vec{E} // \vec{c}$ directions were also studied.

1.2 The Intercalation of Hydrogen into 2H-TaS_2 and 2H-NbS_2 by Electrolysis

Electrolysis is a chemical reaction involving the exchange of charges under the influence of an externally impressed opposed voltage. The intercalation of hydrogen into 2H-TaS_2 by electrolysis was first reported by Di Salvo et al (1973). In our experiment, a piece of single crystal 2H-TaS_2 (or 2H-NbS_2) was used as the cathode and a piece of platinum as the anode. The electrolyte was 1M H_2SO_4.

The reaction at the 2H-TaS_2 (or 2H-NbS_2) cathode can be expressed as

$$\chi H^+ + TaS_2 + \chi e^- \rightarrow H_\chi TaS_2 \qquad (1.2\text{-}1)$$

When a large current is used, the crystal cannot intercalate all of the H, and hydrogen is released at the cathode,

$$2H^+ + 2e^- \rightarrow H_2 \qquad (1.2\text{-}2)$$

and at the anode oxygen is released.

The hydrogen stoichiometry χ in $H_\chi TaS_2$ can be obtained from the number of Coulombs passed through the cell under the condition that no bubbles (H_2) are observed at the cathode. For one mole of electrons, 96500 Coulombs are needed. Note that in in the reduction, one hydrogen ion donates one electron. Thus χ can be calculated from

$$\chi = QM/96500m \qquad (1.2\text{-}3)$$

where Q is the number of Coulombs passed through the cell, M is the molecular weight of the crystal (M_{TaS_2} = 245 g/mole, M_{NbS_2} = 157 g/mole) and m is the weight of the crystal used.

1.3 X-ray Diffraction - Particle Size Effect and Two Dimensional Lattice Reflections

It is well known that X-ray diffraction is an interference effect of the scattered X-ray waves from a crystal. Intense peaks of scattered radiation will be

observed for certain directions where the scattered rays interfere constructively. For a series of parallel lattice planes spaced equal distance d apart, the condition for constructive interference is expressed through the Bragg condition

$$n\lambda = 2d \sin\theta \qquad (1.3\text{-}1)$$

or the Laue condition

$$\vec{k} \cdot \hat{K} = 1/2\ K \qquad (1.3\text{-}2)$$

where the integer n is the order of the corresponding reflection, λ is the wavelength and $\vec{k}$ is the wave vector of the incident X-ray beam, θ is the angle of incidence which is measured from the lattice plane, $\vec{K}$ is the reciprocal lattice vector and K is the length of $\vec{K}$. In all other directions the scattered rays will not be in phase. Furthermore, if the particle size of the crystal is not too small, these rays will be mostly out of phase and cancel each other. Thus the X-ray diffraction pattern will consist of sharp lines at angles satisfying the Bragg law. For small particles, the diffraction lines will be broadened due to the restriction on the number of parallel planes. This broadening is given by the usual expression (Cullity, 1956):

$$B = \frac{0.9\lambda}{t \cos\theta} \qquad (1.3\text{-}3)$$

where B is the broadening of the diffraction line measured at half its maximum intensity(radians), t is the dimension of the particle relevant to the particular reflection being observed and λ and θ have the usual meaning. Note that even for large particles, all diffraction lines have a definite breadth, due to divergence of the incident X-ray beam and sample absorption. While B in Eq. (1.3-3) refers to the broadening due to the particle-size alone. In practice we can use Warren's method[1] to determine B. That is, we can calculate B by using the equation

$$B^2 = B_M^2 - B_S^2 \qquad (1.3\text{-}4)$$

where B_M is the measured breadth and B_S is the standard line breadth for particles with size greater than 1000Å.

[1] See B.D. Cullity, Elements of X-ray Diffraction, p.262, Addison-Wesley (1956).

Usually, if we make a very fine sample (say, sample size less than 0.2 mm in diameter), B_S will be very small and can be neglected (Klug and Alexander, 1954).

According to Klug and Alexander (1954), when the crystallite dimension is less than about 1000Å the K_{α_1}, K_{α_2} doublet becomes unresolvable. At sizes much less than 100Å the back-reflection lines disappear entirely and the low-angles lines become very wide and more diffuse.

Eq. (1.3-3) can be written more explicitly as

$$B_{hk\ell} = \frac{0.9\lambda}{t_{hk\ell}\cos\theta} \qquad (1.3\text{-}5)$$

where $B_{hk\ell}$ refers to the broadening of line $hk\ell$ and $t_{hk\ell}$ is the dimension of the crystal particle along the $[hk\ell]$ direction. For a very thin sheetlike crystallite where the axis c is perpendicular to the sheet, the 00ℓ lines will be broadened while $hk\cdot 0$ lines will remain sharp. When the layers of a layered lattice randomly stack together into parallel groups, a so-called random stacking layer lattice is formed. The diffraction lines from such a lattice are characterized by terminating sharply on the low-angle side and a falling off gradually on the high-angle side. Furthermore, only $00.\ell$ and $hk\cdot 0$ lines will be observed. There will be no general $hk\cdot\ell$ ($\ell\neq 0$) lines (Klug and Alexander, 1954). According to Warren's

calculation (Warren, 1941), the broadening of hk•0 lines in this case should be

$$B_{hk\cdot 0} = \frac{1.84\lambda}{t_{hk\cdot 0}\cos\theta} \qquad (1.3\text{-}6)$$

That is to say two-dimensional lattice hk•0 reflections are broader than three-dimensional lattice hk•0 reflections for the same lateral particle size. Warren has also shown that two-dimensional lattice hk•0 lines are displaced toward larger angles compared to the corresponding three-dimensional case. The amount of this shift is

$$\Delta(\sin\theta) = \frac{0.16\lambda}{t_{hk\cdot 0}} \quad . \qquad (1.3\text{-}7)$$

In the case of truly random orientations of the two-dimensional layers, i.e. if the two-dimensional layers are not parallel to each other or have a random separation, all 00.ℓ lines will be absent and only hk•0 lines will be observed.

Chapter 2

Preparation and Structure Determination of Single Layer TaS_2 and NbS_2

2.1 Preparation of Single Layers

The idea of monodispersing 2H-TaS_2 by a technique involving the intercalation of hydrogen and then water was first described by Murphy and Hull (1975). The technique described here uses the same basic idea with some improvements described below.

Single layers were made from single crystals 2H-TaS_2 and 2H-NbS_2. These crystals were previously grown in our laboratory from high purity elements by vapor phase transport with iodine as a transport agent. Hydrogen is intercalated into 2H-TaS_2 (NbS_2) layers electrolytically in 1M H_2SO_4 as shown in Fig. 2.1. The crystal cathode was held by a platinum clip and a piece of platinum sheet was used as the anode. A Princeton Applied Research model 173 Potentiostat/Galvanostat was used as a power supply and was operated in mode of "Current Control". For a crystal of 2mg to 4mg, typically 4mm × 5mm × 0.02mm in size, a current of 50μA to 80μA was usually used. The potential between the two electrodes as monitored by a AVO meter, was around 1.65V at the beginning and increased gradually to 2V four hours later. The electrolysis lasted for

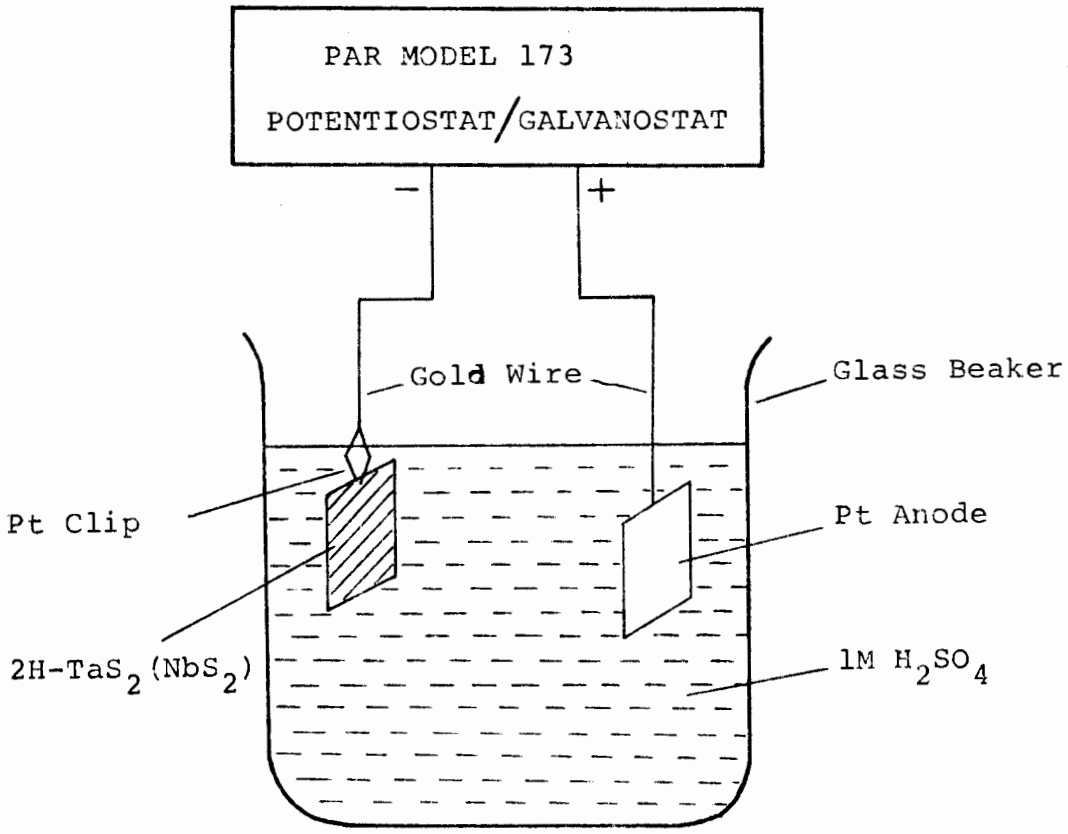

Fig. 2.1: Set-up for intercalating hydrogen into the layered crystals.

about four hours and was ended by a sharp increase in current of about 50mA to 80mA (the potential went up to about 3V correspondingly) for a fraction of a second. Violent bubbling was observed in both electrodes when the current was increased. Immediately following this, the crystal was taken out of the acid and put into deionized water where a tremendous expansion (> 30 times) could be observed. The thickness mesurements were made both before and after the expansion under a microscope. The surface of the expanded crystal became silvery while the inside part was dark brown in color. Immediately, the inside part of the expanded crystal was put into a test tube with about 5cc of deionized water and then was broken up into a uniform suspension by placing in a BRANSON B-12 ultrasonic cleaner. The breaking up of the expanded crystal was very fast (just a few seconds) when the test tube was inserted in the resonant region of the ultrasonic cleaner. A colored suspension was thus obtained. It is shown below that such suspensions consist of freely floating single layers.

Concentrated single layer suspensions of both TaS_2 and NbS_2 are dark brown in color. A dilute suspension of TaS_2 is yellow-brown in transmission (for $\sim$1cm path length) while that of NbS_2 is also yellow-brown but somewhat reddish. It was observed that single layers of TaS_2 in suspension tend to

flocculate. Dilute suspension of TaS_2 can last for about one hour without noticeable flocculation. The suspension usually became clear after about a day as the floccules settled to the bottom of the test tube. The NbS_2 single layer suspension was observed to be much more stable with regard to flocculation. Dilute NbS_2 single layer suspensions can last for more than one week without flocculation. Some precipitate of NbS_2 will appear at the bottom of the test tube during that time but the suspension will still be colored. This precipitate of NbS_2 is readily re-suspended in the ultrasonic cleaner, while the floccules of TaS_2 cannot be re-suspended ultrasonically.

A slight odour of hydrogen sulphide emanates from fresh TaS_2 water suspension which becomes quite strong after a few days. However, for NbS_2 suspension, no such odour was smelt even if the suspension lasted for weeks.

As mentioned in the paper by Murphy and Hull (1975), adding surfactant (surface active agents) such as glycerol and Triton X-705 to TaS_2 single layer suspensions can increase the electrostatic repulsion between layers and reduce the van der Waals attractive forces and thus stabilize suspension for several days. In our experiment, 1% Triton X-705 was added into a yellow-brown TaS_2 single layer suspension for the optical measurements. For NbS_2, no surfactant was used.

Crystals in the suspension can be easily removed from the

suspension by centrifugation. For a dilute yellow brown TaS_2 single layer suspension, a 15 minutes centrifugation at 3000 rpm ($\sim$1500 g's) brought most of the crystals to the bottom of the test tube and the suspension became light yellow in colour. For NbS_2 a dilute yellow brown coloured suspension became light yellow-brown after 15 minutes centrifugation at 3000 rpm.

When the same method was applied to semi-conductor 2H-MoS_2 no expansion was observed and the crystal remained the same colour and thickness as before electrolysis. For 2H-$NbSe_2$ and 1T-TaS_2, although a large expansion of the crystals was observed after electrolysis, the expansion was not uniform in the sense that the crystals were expanded to split platelets and these platelets were not "soft". Under a microscope the expanded crystal was observed from its edges and many thinner platelets were seen indicating that water did not uniformly intercalate. The X-ray pattern of such crystals showed the normal 2H structure with no two-dimensional character. Various current densities and different concentrations of the electrolyte were tried without success.

2.2 X-ray Powder Photography of Single Layers

The single layer forms of TaS_2 and NbS_2 were mainly

determined by X-ray powder photography. Nickel filtered CuK_α radiation, a Debye-Scherrer camera of 57.3 mm in diameter, and a 1 kw X-ray machine (Phillips Electronic Instruments, Mount Vernon, N.Y.) were used. X-ray photography was carried out for several sample forms as described below. Although the following description concerns only TaS_2, similar results were also obtained for NbS_2.

2.2.1 X-ray Powder Photography of the Water-Expanded Crystals

The crystals of 2H-TaS_2 and 2H-NbS_2 are tremendously expanded after intercalation of hydrogen and water. We call this form the "expanded crystals". They are very "soft" in the sense that when they are removed from water they take the form of a drop due to the surface tension. These water-expanded crystals were observed to deintercalate water even if they were still immersed in water. The deintercalation of water from the expanded crystals was rather fast: the "soft" expanded crystals started to "harden" in about an hour. When they were hardened they did not change their form when they were removed from water. The implication is that "hardened" crystals are deintercalated of water. In order to record the crystal structure before deintercalation of water, X-ray powder photographs were carried out immediately after that the crystals were expanded. Furthermore, to prevent water evaporation, the X-ray sample holder was made in a special way as shown in Fig. 2.2. A thin wall glass capillary was fixed

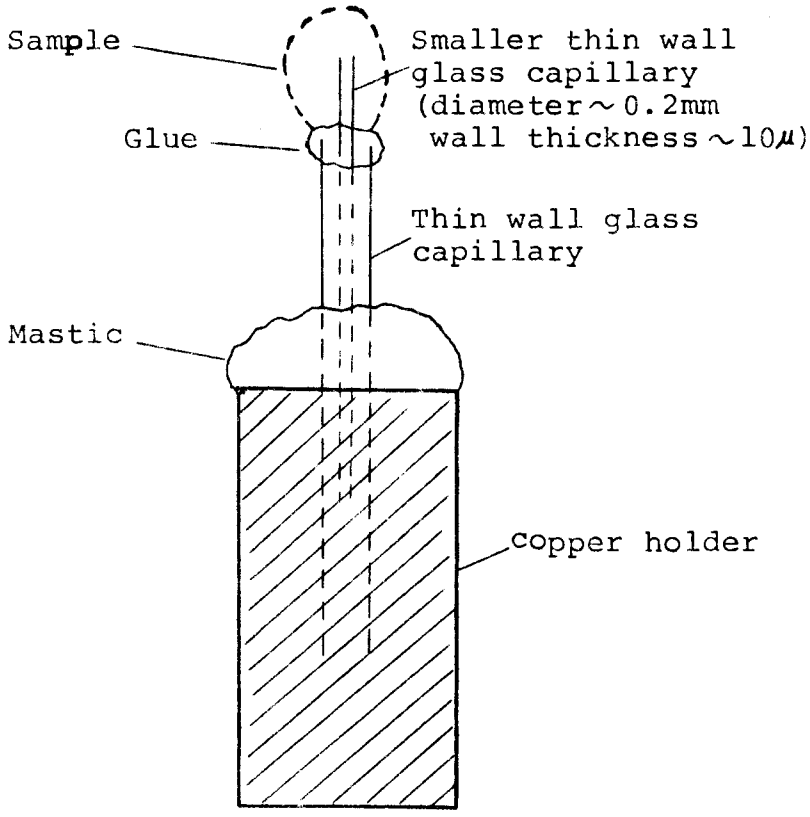

Fig.2.2: X-ray sample holder for studying the "soft" water-expanded crystals.

in the hole of a copper holder. Another smaller thin wall glass capillary $\sim$0.2mm in diameter and of $\sim$10 μ wall thickness was inserted and fixed with glue. The thin wall glass capillaries were made from glass tubing by heating the tubing in flame followed by a rapid pulling. The inside part of the expanded crystal was carefully selected by using two pairs of tweezers and mounted around the smaller capillary. It was then held there by surface tension.

The exposure of X-rays lasted for only 20 minutes under the condition of 30 kV cathode-anode potential and 29 mA current. The X-ray pattern obtained for water-expanded crystals is shown in Fig. 2.3(b). The two-dimensional character of the expanded crystals is evident and will be discussed later.

For comparison Fig. 2.3(a) shows an X-ray photograph of a powder made from the original 2H-TaS_2 single crystal. Fine particles of the single crystal were obtained ultrasonically. The X-ray sample holders used for dry powders were similar to that shown in Fig. 2.2 but a fine glass fibre was used instead of the smaller capillary and nail polish or grease was needed

Fig.2.3: X-ray diffraction patterns for

(a) Original 2H-TaS_2 crystal

(b) Water-expanded TaS_2 (immediately after intercalation of water)

(c) TaS_2 after deintercalation of water.

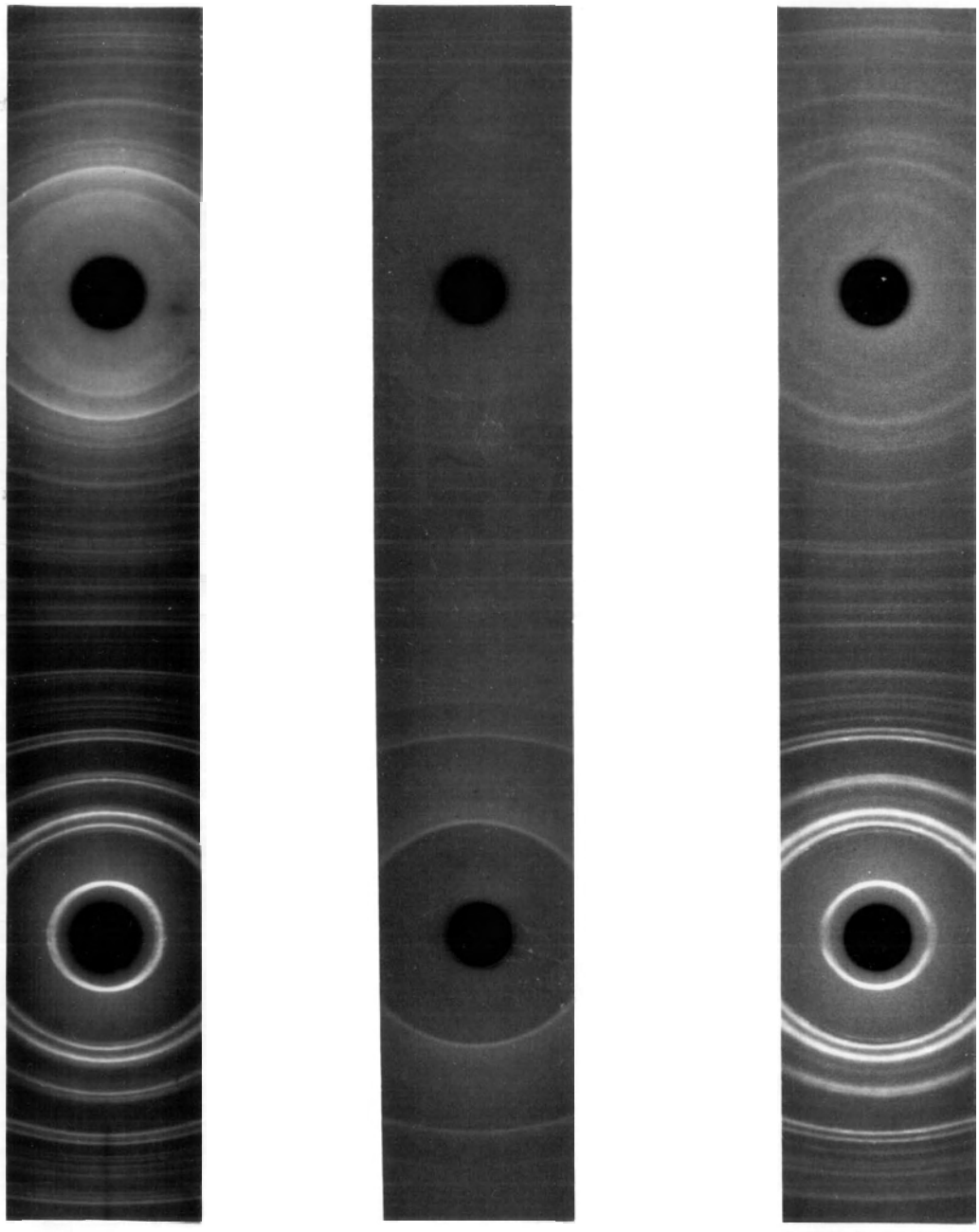

(a) (b) (c)

to mount the powders. The exposures for dry powders usually took one hour under the condition of 40 kV cathode-anode potential and 20 mA current.

2.2.2 Deintercalation of Water from the Expanded Crystals

The deintercalation of water from the "soft" water-expanded crystals was observed both from the X-ray patterns and the appearance of the expanded crystals.

The pattern for a 35 minutes exposure for the "soft" water-expanded crystals is shown in Fig. 2.4. Some very short arc lines in the low angle region are seen. This indicates that the expanded crystal was beginning to dry, or deintercalate water. To verify this, another experiment was carried out. An X-ray sample of the "soft" expanded TaS_2 was made as before. Two sequential exposures, each of 20 minutes, were made for the same sample. The second exposure was carried out immediately after the X-ray film was replaced. An X-ray pattern like Fig. 2.3(b) was obtained for the first exposure and the second exposure gave a pattern like that shown in Fig. 2.4.

As seen from the appearance, the expanded crystals restacked together after deintercalation of water. When an expanded crystal was taken out of water, it reverted to its

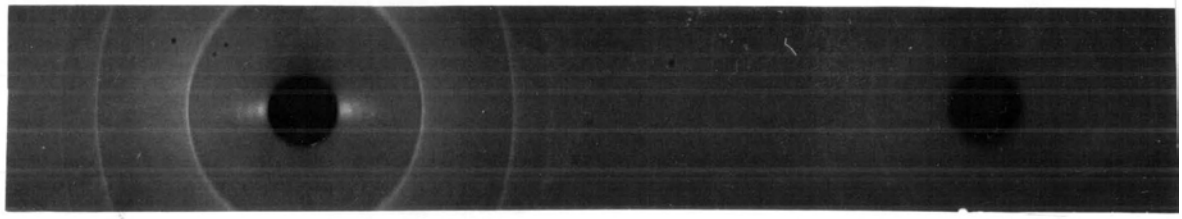

Fig.2.4: X-ray diffraction pattern of a "partially dried" expanded TaS_2 crystal.

original thickness on drying out. When an expanded crystal dried, it was found that they could not be expanded again by adding water, in contrast to the observations of Murphy and Hull (1975).

The dried restacking TaS_2 crystal was broken into fine powders by using an ultrasonic cleaner and its X-ray pattern is shown in Fig. 2.3(c).

When an expanded crystal was kept in water for an extended time (> 1 hour) it kept the expanded size but became "hard" - that is, split platelets could be seen at the edge and could be separated apart by using tweezers. The inner platelets had also a silvery surface. By contrast, the inside part of the "soft" expanded crystal was dark brown in color. The X-ray pattern of the "hardened" platelets showed (00.ℓ) lines as well as hkℓ($\ell \neq 0$) lines, indicating that these platelets were partially dried out. These platelets could not be re-suspended ultrasonically.

It was found that the silvery surface part of the "soft" expanded crystal was also difficult to suspend ultrasonically, implying that the deintercalation of water from the expanded crystal occurs first at the surfaces of the crystal.

2.2.3 Re-stacking of Dried Single Layers

Several drops of the single layer TaS_2 suspension in

water were allowed to dry on a clean microscope slide and repeated adding and drying of the suspension 3 times on the same place was carried out. This material was scraped from the glass and its X-ray pattern is shown in Fig. 2.5(a). Repeated adding and drying of the suspension up to 15 times formed a thin film about 1000Å thick (as estimated from its brown color). The X-ray pattern of this thin film as shown in Fig. 2.5(b) shows slight difference compared with Fig. 2.5(a).

A photograph recording drying of the single layer TaS_2 suspensions on a microscope slide is shown in Fig. 2.6. The shining part shows the crystal. The small inner circle area shows that another small drop of suspension was added on the background of the first dried crystal. It can be seen that the suspension dried on glass non-uniformly and the dried crystal is uneven in thickness.

An X-ray photograph was also made for the deposits of TaS_2 single layer suspension obtained by centrifugation at 2000 rpm ($\sim$650g's) for 20 minutes. The pattern is shown in Fig. 2.5(c) and will be discussed later.

2.2.4 Effects of $AgNO_3$ Water Solution on Single Layer Suspensions

It is well known that silver atoms intercalate into

Fig.2.5: X-ray diffraction patterns for

(a) the random stacking single layer TaS_2 crystal obtained by drying single layer suspension on glass for 3 times

(b) drying suspension on glass for 15 times

(c) the centrifuged deposit of single layer TaS_2 suspension.

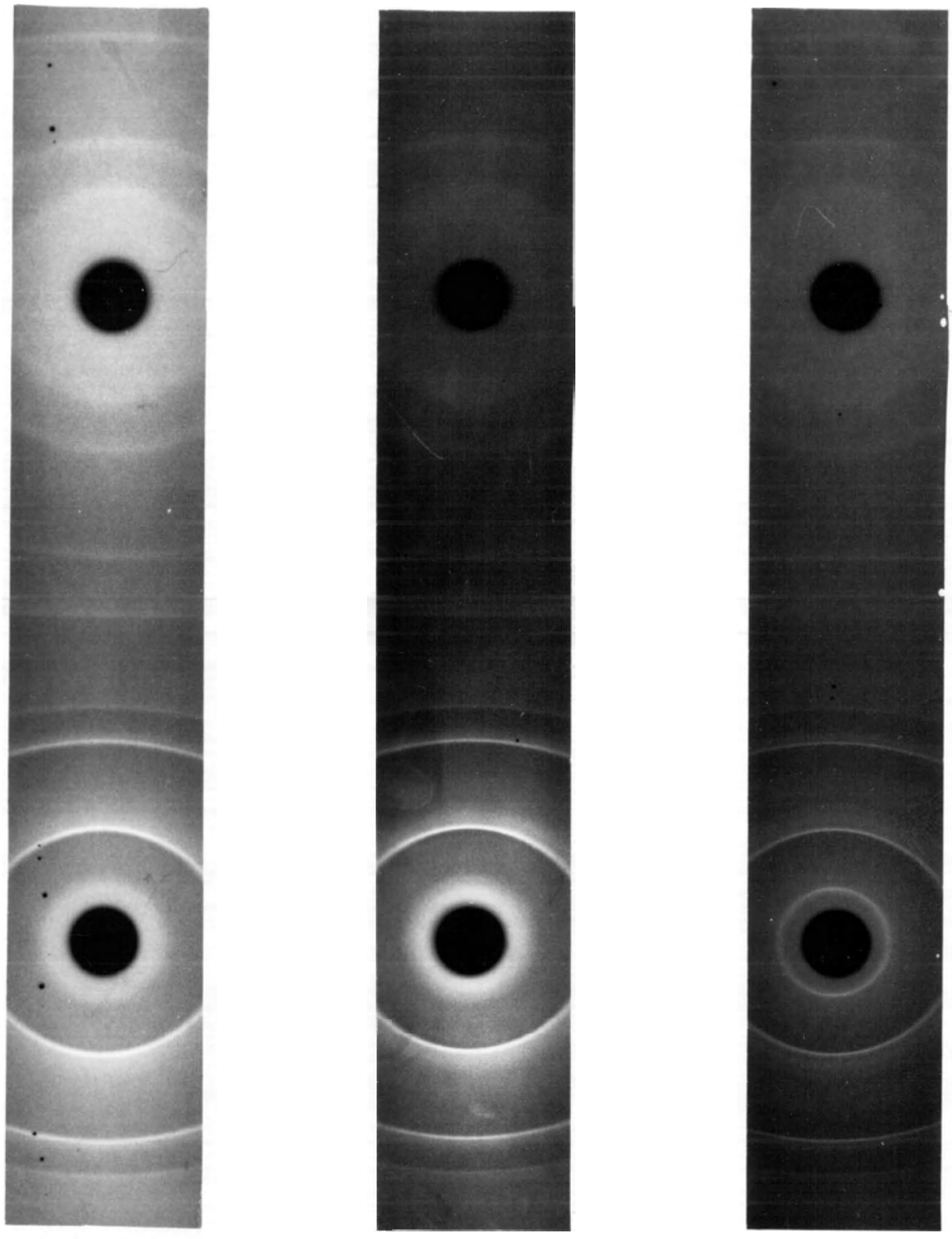

(a) (b) (c)

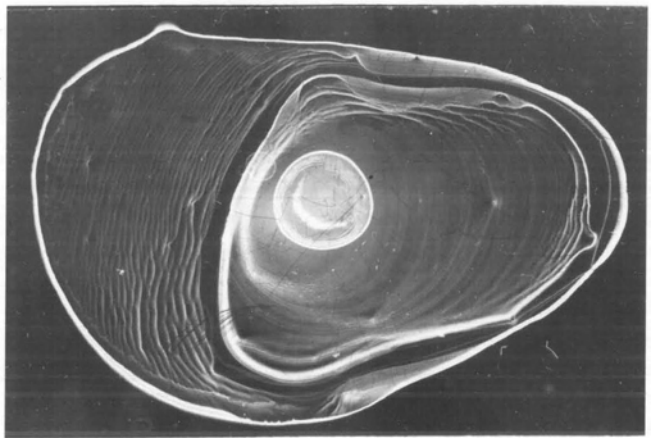

Fig.2.6: TaS_2 single layer suspension dried on a microscope slide.
Magnification: about X2.

2H-TaS_2 crystal when TaS_2 is placed in $AgNO_3$ solutions, and a variety of ordered superlattices are observed for the Ag-TaS_2 system (Scholz and Frindt, 1980). To see what would happen if we added silver ions to the single layer TaS_2 suspension, the following experiment was carried out. One drop of 0.1M $AgNO_3$ water solution was added to 2cc of yellow-brown single layer TaS_2 suspension. A dark trace was observed as soon as the $AgNO_3$ solution was added. After a few seconds the suspension began to flocculate and settle to the bottom of the test tube. The flocculate was washed with water and then dried and its X-ray pattern, quite different from the original TaS_2 pattern, was shown in Fig. 2.7(a).

The same experiment was carried out for NbS_2. This time some floatage appeared on the surface of the suspension instead of settling to the bottom of the test tube after the $AgNO_3$ solution was added. The X-ray pattern of the floatage (Fig. 2.7(b)) is again different from the NbS_2 patterns and different from Fig. 2.7(a). We will discuss this later.

2.3 Electron Microscopy of Single Layer TaS_2

To determine the lateral size and observe the electron diffraction pattern of single layers, electron microscopy

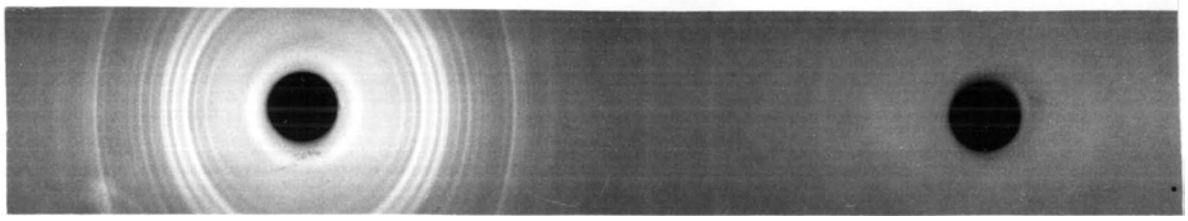

(a)

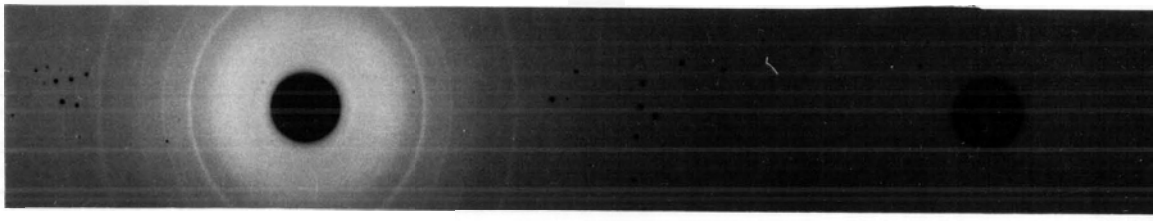

(b)

Fig.2.7 X-ray diffraction patterns for
(a) deposits of "single layer TaS_2 suspension + $AgNO_3$ solution",
(b) floatage of "single layer NbS_2 suspension + $AgNO_3$ solution".

studies were carried out for single layers of TaS_2.

The sample used for these studies was prepared as follows: A 200 mesh copper electron microscope grid covered with a thin carbon film about 100Å thick was used as the sample holder. A yellow-brown single layer TaS_2 suspension was centrifuged at 3000 rpm ($\sim$1500g's) for 15 minutes. The suspension then became light yellow in color. A small drop of this light yellow suspension was put on the sample holder by using a glass capillary and removed immediately by another empty capillary. By this means very small amounts of crystal were deposited on the carbon film. The samples were examined in a Phillips EM300 electron microscope by Dr. O. Singh under a magnification of 1.2×10^5. Many thin crystal platelets with a lateral size from 500 to 3000Å were seen. Some of the platelets were overlapping.

The crystals were so thin that they were rather difficult to see in the electron microscope. But still, they were identified from the contrast and were distinguished from carbon film by checking their electron diffraction pattern. According to the contrast vs. thickness measurements made by Dr. O. Singh, the fairly visible TaS_2 platelets had thickness values of ca. 15Å and for the thinnest ones, the changes in transmitted intensity were not measurable. These thinnest

Fig.2.8: (a) Electron microscope photograph of a TaS_2 platelet probably two layers thick (Magn. X 1.2×10^5).

(b) Electron diffraction pattern of the TaS_2 platelet shown in (a), temperature 25°K.

(taken by Dr. O. Singh).

(a)

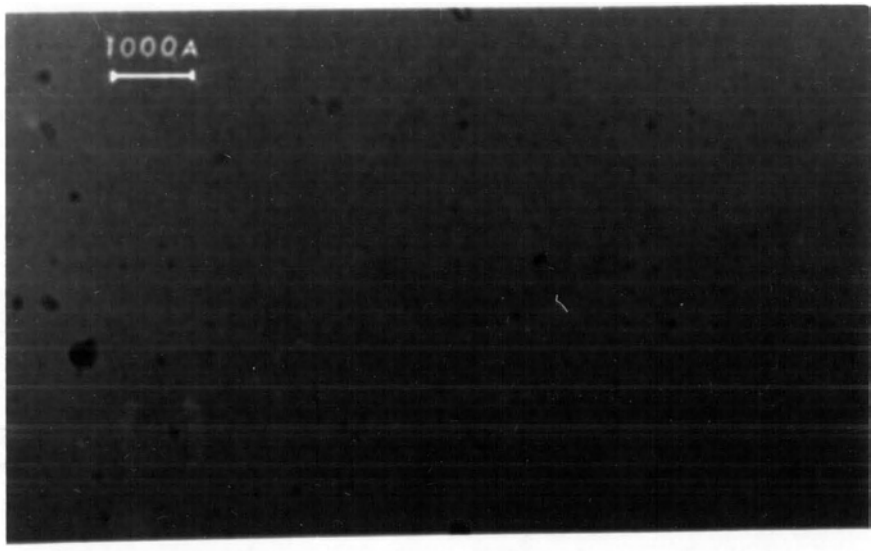

(b)

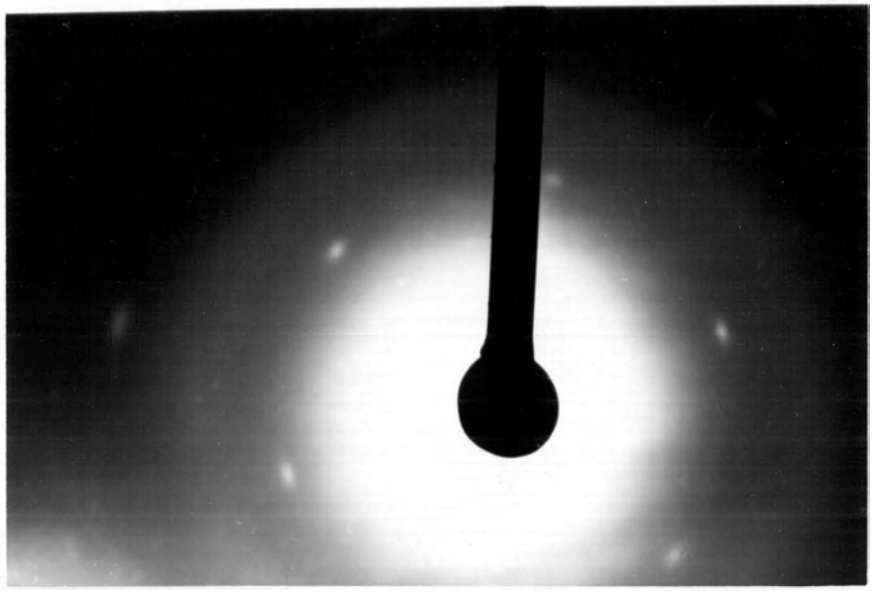

platelets are likely single layers. An electron microscope photograph of a TaS_2 platelet probably two layers thick is shown in Fig. 2.8(a). The electron diffraction pattern of the platelet is shown in Fig. 2.8(b).

No charge density wave superlattice was observed for such TaS_2 platelets when they were cooled down to about 25°K.

2.4 Analysis of the X-ray Results

2.4.1 Indexing and Intensity Calculations of Original 2H-TaS_2 Crystal Diffraction Pattern

The X-ray diffraction pattern of the original 2H-TaS_2 crystal powder is shown in Fig. 2.3(a). The pattern lines were indexed using the analytical method introduced in the book by Cullity (1956). This indexing was checked by comparing the measured line positions and the calculated line positions according to the published data of the lattice parameters of 2H-TaS_2 (a = 3.315Å, c = 6.05 × 2Å, Jellinek (1962)). It was also checked by comparing the observed diffraction line intensities and the theoretically calculated intensities. The calculated line intensities and the observed ones are compared in Table 1. The calculation was carried out using the following formula given in Cullity's book:

$$I = p \frac{1 + \cos^2 2\theta}{\sin^2\theta\cos\theta} |F|^2 \qquad (2.4\text{-}1)$$

hkl	$I_{calc.}$	$I_{obs.}$
002	98	VS
004	7	VW
100	38	S
101	8	VVW
102	100	VS
103	6.6	VVW
104	88	VS
006	8.9	VW
105	3.4	VVW
110	36.5	S
106	33	S
112	32	S
008	9.6	W
200	7.6	VW
108	12	W
202	22.8	W
204	31	W
116	20	W
118	31	S
210	8.6	VW
208	8.3	VW
11.10	14.2	W
300	7	VW
220	11.7	VW
308	60.6	S
310	22	W

Table 1: Calculated and observed intensities for pure 2H-TaS_2 X-ray diffraction lines.

where I is the relative integrated line intensity in arbitrary units, $\mathfrak{p}$ is the multiplicity factor, its values for group D_{6h} crystals are given below (Klug and Alexander, 1954):

Index	hkℓ	hhℓ	h0ℓ	hk0	hh0	h00	00ℓ
Value of p	24	12	12	12	6	6	2

and F, the structure factor, is expressed as

$$F = \sum_j f_j \, e^{2\pi i(hx_j + ky_j + \ell z_j)} \qquad (2.4\text{-}2)$$

and calculated by using the unit cell shown in Fig. 1.3. The atomic form factor f is treated as a constant here and $f_{Ta} \approx 4.5\, f_S$ is used according to the atomic number of Ta and S atoms. The values of the Bragg angle θ are from the observed positions of each hkℓ line.

The indices of some main diffraction lines are shown in Fig. 2.9. For clarity, some very very weak (vvw) lines and the doublets in the high angle region are not shown. The height of the lines in Fig. 2.9 indicates the relative diffraction intensity qualitatively. By combining the technique of Straumanis (1940) and the extrapolation method introduced in the book by Klug and Alexander (1954) the

Fig.2.9: X-ray diffraction pattern lines for

(a) the original 2H-TaS_2

(b) the "soft" water-expanded TaS_2

(c) TaS_2 after deintercalation of water.

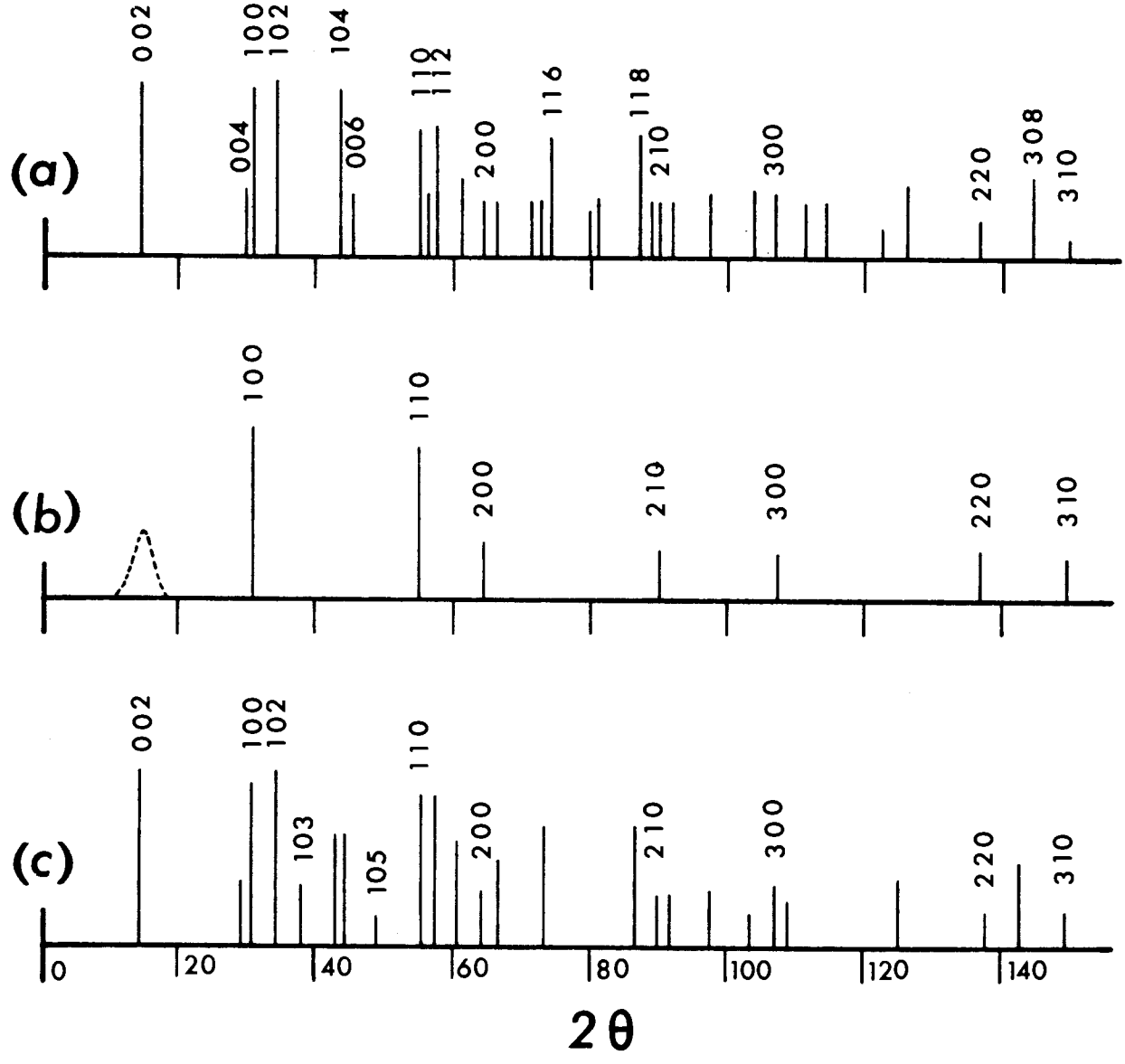
(a)
002
004
100
102
006
104
110
112
200
116
118
210
300
220
308
310
(b)
100
110
200
210
300
220
310
(c)
002
100
102
103
105
110
200
210
300
220
310
0
20
40
60
80
100
120
140
2θ

lattice parameters of our 2H-TaS_2 crystal were determined as a = 3.313 ± 0.005Å and c = 12.11 ± 0.02Å, which are very close to published results (Jellinek, 1962). In the work of lattice parameter determination, a very fine X-ray sample (~0.2 mm in diameter) was used and carefully centered in the camera, and good-quality lines in the back-reflection region were utilized.

The same methods were used to index diffraction lines and calculate the theoretical line intensities for 2H-NbS_2. Since the results are essentially similar they are omitted here, except to report that the lattice parameters a= 3.311 ± 0.005Å and c = 11.95 ± 0.02Å, are in good agreement with published results.

2.4.2 The "Soft" Water-Expanded TaS_2 Crystal

From Fig. 2.3(b) and Fig. 2.9(b) we can see that the "soft" water-expanded crystal gave no 00ℓ lines and no hkℓ (ℓ≠0) mixed lines. After deintercalation of water the crystal gave a pattern similar to the original 2H-TaS_2 pattern. The positions of hk•0 lines for either "soft" water-expanded crystal or after its deintercalation of water have no noticeable change. This indicates that there is no significant change in the layer a-axis to within ~1%. Details will be discussed later.

2.4.3 The "Partially Dried" Expanded TaS_2 Crystal

In the pattern for the partially dried or partially deintercalated expanded TaS_2 crystal shown in Fig. 2.4, the short arcs in the low angle region can be identified as 00ℓ lines since the arc shape shows the preferred orientation of the layers of the crystal. Since these lines are broad and unclear, it is difficult to measure their positions accurately, however, four lines at θ angles of 4.8°, 6.0°, 7.25° and 8.95° were measured and identified as (008), (00.10), (00.12) and (00.14) lines. Thus the spacing between neighboring layers was estimated to be ca. 37Å. This spacing is about 6 times the initial spacing of 2H-TaS_2. It follows from this estimation and the observed extent of crystal expansion (> 30 times) that we can safely say that before deintercalation of water the average spacing between neighboring layers of the "soft" water-expanded crystal is more than 100Å.

2.4.4 Dried Single Layers and Centrifuged Deposits From Single Layer TaS_2 Suspension

The X-ray diffraction pattern of the random stacking single layer TaS_2 obtained by drying single layer suspensions on glass for 3 times (Fig. 2.5(a)) shows a very wide (002)

line in the low angle region. It implies that the particle size along the c axis is very small. It is hard to determine the line width because part of the line falls into the punch hole region. In spite of this, the pattern indicates that the particle size along the c axis is only a few layers thick. This follows from the width of the (002) line and Eq. (1.3-3). The average c spacing between layers was estimated as 6.3Å according to an estimate of the central position of the observed (002) line. This spacing is slightly bigger than the spacing of 2H-TaS_2 ($c_o \approx 6.05$Å, $\Delta c/c_o \sim 4\%$). The positions of the (hk•0) lines in Fig. 2.5(a) are slightly displaced toward large angles compared with the original 2H-TaS_2 pattern. For the (110) reflection $\Delta(\sin\theta) \approx 0.0016$ and the original $\sin\theta_o = 0.463$, the displacement amounts to 0.35%. This displacement is consistent with Warren's argument (see Eq. (1.3-7)) and confirms the two-dimensional character of the sample.

In the case of drying suspension on glass for 15 times, the corresponding X-ray pattern (Fig. 2.5(b)) still shows a wide (002) line despite the fact that the dried crystal film was as thick as more than 1000Å. The average c spacing between layers was estimated as 6.15Å which is also bigger than the spacing of 2H-TaS_2 but is smaller than that in the case of 3 times drying. It was noticed that the displacement of (hk•0) lines toward large angles in Fig. 2.5(b)

($\Delta(\sin\theta)/\sin\theta_o \sim 0.17\%$) is slightly smaller than in Fig. 2.5(a). As a whole, Fig. 2.5(a) and Fig. 2.5(b) are similar. No higher order (00ℓ) lines can be observed in both patterns.

The dried deposit from the suspension obtained by centrifugation gave an X-ray pattern which shows a sharp (002) line (Fig. 2.5(c)). Other higher order (00ℓ) lines are too weak to be seen, however, seven (hk•0) lines are easily seen in the pattern. A displacement of (hk•0) lines is not detectable here. Other diffuse rings indicate that some ordering between layers occurs when the single layers stack together.

2.4.5 Effects of Adding $AgNO_3$ to Single Layer Supsensions

The addition of $AgNO_3$ water solution has an interesting effect on a single layer TaS_2 suspension. X-ray analysis shows that the dark flocculates which appear are a mixture of single layer TaS_2 and silver sulphide (Ag_2S). The positions and intensities of the observed lines up to $2\theta = 65°$ are tabulated in Table 2 and compared with Graham's[2] data for Ag_2S. In Table 2 the line positions are expressed in

[2]See Standard X-ray Diffraction Powder Patterns, NBS Circular 539, 10, 51 (1960).

Graham (1949) Cu 1.5418A		Our data Cu 1.5418A		Indices	
				Ag_2S	TaS_2
d(A)	I	d(A)	I	hkl	hk0
3.45	10	3.43	VVW	111	
3.38	5	-	-	012	
3.09	30	3.09	W	111	
2.85	40	2.87	VS	112	100
2.67	20	2.67	VVW	120	
2.60	100	2.59	S	121	
2.45	80	2.45	S	112	
2.38	50	2.38	W	103	
2.22	30	2.23	W	031	
2.09	40	2.09	W	122	
2.04	5	-	-	103	
2.00	5	2.00	VVW	131	
1.96	10	1.97	VW	123	
1.91	10	1.91	VW	131	
1.87	10	1.86	VW	014	
1.72	30	1.73	W	213	
1.69	5	-	-	041	
		1.66	S		110
1.58	20	1.59	VW	141	
1.54	10	1.54	VVW	105	
1.51	10	1.52	VVW	015	
1.46	20	1.46	VVW	134	

Table 2: X-ray data for the deposits of "single layer TaS_2 suspension + $AgNO_3$ solution" compared with the published data of Ag_2S (monoclinic).

distances between neighboring planes. Our data for all the lines except the TaS_2 hk0 lines fit quite well with Graham's data for both "distance" and "intensity".

In Fig. 2.7(a), there is a broad diffuse ring in the low angle region indicating the stacking of parallel crystal layers. The average spacing betwen layers was estimated as 6.33Å.

Experiments showed that there is a minimum amount of $AgNO_3$ solution required to remove all TaS_2 crystals from suspension. This minimum amount of $AgNO_3$ depends on the concentration and quantity of single layer suspensions. In our experiment one drop of 0.1M $AgNO_3$ water solution was just able to remove almost all TaS_2 crystals from a 2cc yellow-brown single layer suspension and the suspension became very light yellow. When one drop of 0.05M $AgNO_3$ was added to 2cc the same kind of yellow-brown suspension, the suspension remained light yellow-brown in color, indicating that there were still single layers TaS_2 in the suspension. When two drops of 0.1M $AgNo_3$ solution was added to a 2cc yellow-brown suspension, the suspension became totally clear and its flocculate gave an X-ray pattern which contained silver crystal lines in addition to Ag_2S lines and TaS_2 hk0 lines.

The same experiment for NbS_2 single layer suspension showed a different result. Instead of producing a flocculate which settled to the bottom, some floatage appeared on the

surface of the suspension after adding $AgNO_3$ solution. The floatage gave an X-ray pattern containing NbS_2 (hk•0) lines and silver crystal lines, but no Ag_2S lines were observed.

These observations suggest that the Ag_2S results from a reaction of silver and sulphur arising from some decomposition of TaS_2 during the preparation of the single layers. There is no indication that such decomposition occurs in the preparation of NbS_2 single layers. It is unlikely that Ag ions have seized S ions from TaS_2 directly, since in the X-ray pattern (Fig. 2.7(a)) TaS_2 (hk•0) lines are still rather strong and the line positions have no noticeable change, and besides, no Ta crystal lines are observed. To confirm the above analysis, an atomic analysis experiment is needed.

2.5 Effects of the Sharp Increase in Current in Electrolysis

A special technique presented in this thesis is the use of a current pulse at the end of electrolysis for a fraction of a second, the so-called "electric shock" technique. The effects of using and not using this technique have been studied and several differences in these two cases have been found.

First of all, it was found that without the current pulse the crystal was less expanded after electrolysis and immersion into water. It was also found that even though the expanded crystal was also "soft", the process of the expansion was much

slower. More importantly, the expansion was not uniform, and a larger expansion was observed at the crystal edges. A schematic sectional diagram of such an expanded crystal is shown in Fig. 2.10(a). By contrast, when the current pulse was used, an almost immediate uniform expansion was always observed.

Secondly, the X-ray diffraction patterns of the "soft" water-expanded crystal obtained with and without the use of the "electric shock" technique are also different. The pattern for a sample obtained with the "shock", shown in Fig. 2.3(b), shows (hk.0) lines only. While in the pattern for a sample obtained without the "shock", as shown in Fig. 2.10(b), diffuse hk•ℓ ($\ell \neq 0$) lines are also seen. Different current densities and electrolysis times have been tried without using "electric shock" but none of them could give an X-ray pattern as neat as Fig. 2.3(b). This indicates that the "electric shock" technique does help to get hydrogen and water intercalated into every van der Waals gap.

Finally, in both cases, a uniform suspension was readily obtained by ultrasonic treatment and both dilute centrifuged top suspension showed very low contrast platelets in the electron microscope. However, it was observed that the suspension usually flocculated quickly (within 2 hours) for the platelets made without using the "electric shock". With the "electric shock", the particles remained in suspension

Fig.2.10: (a) A schematic sectional diagram showing the uneven expansion for a partially water intercalated crystal (no shock treatment).

(b) A typical X-ray pattern of the "soft" expanded crystal without using "electric shock" technique.

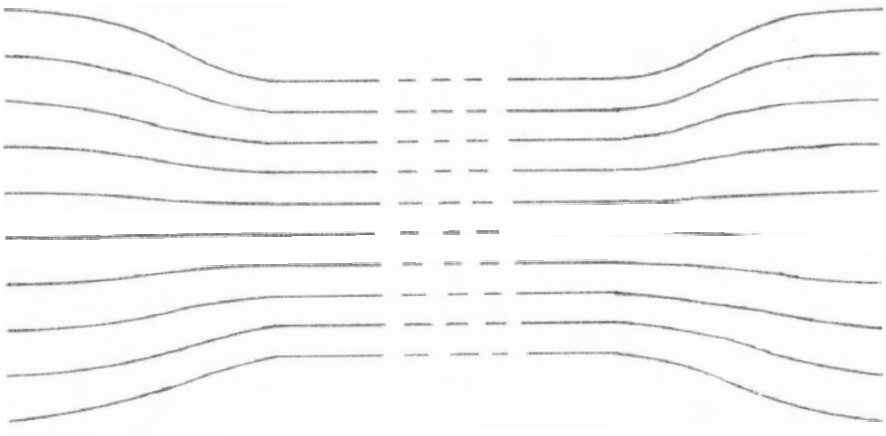

(a)

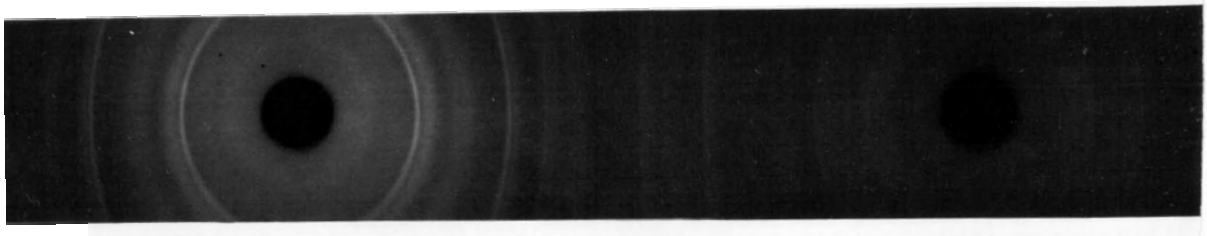

(b)

overnight or even longer. This implies that the crystal layers in suspensions produced with the "electric shock" are more thoroughly separated.

The mechanism of the so-called "electric shock" is not clear, but it is thought that the violent charge transfer and hydrogen bubbling within the crystal is responsible for the uniform thorough intercalation of hydrogen and water. It is of interest to note that the "electric shock" does not destroy the crystal structure. This is confirmed by the fact that the expanded crystal restacks back to 2H structure after the deintercalation of water and also by the observation that the a parameter did not change after the water-expansion.

2.6 Discussion

The tremendous expansion and the X-ray powder pattern of the "soft" water-expanded crystal (Fig. 2.3(b)) give the strongest indication that the single layer form of the crystals can be obtained by dispersion into suspensions. The absence of the (00.ℓ) and hk•ℓ ($\ell \neq 0$) lines and the integrity of the (hk•0) lines allow us to propose a model of the "soft" water-expanded crystal -- as intact single layers of crystal greatly separated by water. The great expansion of the crystal on intercalation with water and the X-ray data for "partially dried" crystals indicate that the layer separation is greater than 100Å. The presence of such large amounts of

water between the layers greatly reduces the strength of the inter-layer bonding so that single layer suspensions are readily obtained by a small amount of ultra-sonic dispersion.

The absence of all the $\ell \neq 0$ lines in Fig. 2.3(b) indicates that water molecules have intercalated into every van der Waals gap. It is easy to show (Klug and Alexander, 1954) that for a group of N parallel layers the scattering profile of a (00·ℓ) reflection is of the form

$$I = \frac{\sin^2 \frac{2\pi N d \sin\theta}{\lambda}}{\sin^2 \frac{2\pi d \sin\theta}{\lambda}} \qquad (2.6\text{-}1)$$

where I represents the intensity, other symbols have the same meaning as that in Eq. (1.3-1). From this expression as well as from the physical meaning of X-ray diffraction we can see that the peak intensity decreases and the line width increases as N decreases. For N = 2, (00·ℓ) lines get maximally broadened and for N = 1, i.e. single layer groups, there will be no (00·ℓ) lines. By using Eq. (2.6-1) for two-layer groups of TaS_2, the scattering profile of the (002) reflection was obtained and is shown in Fig. 2.11. Since for 2H-TaS_2 the relative intensity of the (002) reflection is high (about 2.6 times higher than (100) and ~3 times higher than (110)

Fig.2.11: Scattering profile of (002) reflections for hypothetical two-layer groups of TaS_2.

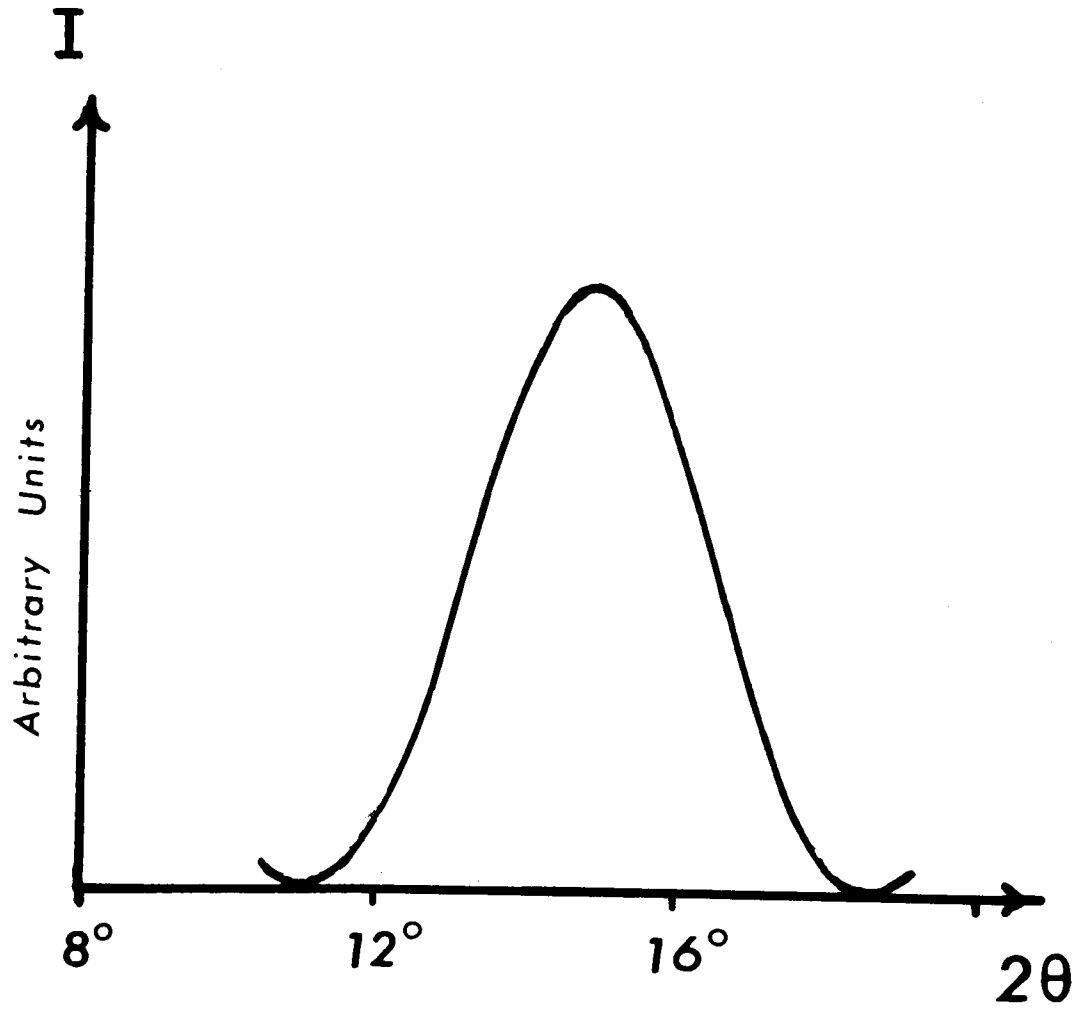
I
Arbitrary Units
8°
12°
16°
2θ

reflection) if the "soft" water-expanded TaS_2 crystal contains significant numbers of two-layer groups, a broad (002) line should appear in the X-ray pattern as shown by the dashed curve in Fig. 2.9(b). No evidence for (002) scattering is seen in Fig. 2.3(b) so that we can conclude that the sample contains no significant number of two-layer or other multi-parallel-layer groups. We can thus call the pattern shown in Fig. 2.3(b) the "single layer X-ray pattern". Observations on many patterns for both TaS_2 and NbS_2 agree with this conclusion.

The X-ray patterns of the TaS_2 partially dried layers (Fig. 2.4) and totally dried layers (Fig. 2.3(c)) confirm the above model, whenever there is a regular c spacing. There are always some (00·ℓ) lines in the low angle region. As the water deintercalates, the crystal restacks back to the original 2H structure with some stacking faults and distortion as indicated by the increasing intensity of the (103) and (105) lines and other changes in the high angle region (Fig. 2.3(c)).

In all cases the a parameter of the layers remained unchanged to within one percent, as determined from the positions of (100), (110) and (200) lines. These lines are not significantly broadened indicating that the bonding within a layer is very strong and the lateral dimensions of the layers are at least 300Å.

In the case of heat treated carbon blacks, Warren (1941) showed that carbon blacks are built up from individual graphite layers arranged parallel to one another at about the normal graphite spacing but are random in translation parallel to the layer and rotation about the normal. The X-ray powder pattern for such material consists of two kinds of reflections -- normal crystalline type (00•ℓ) reflections and diffuse two-dimensional lattice (hk•0) reflections which are characterized by line asymmetry, the line rising sharply on the low-angle side but falling off gradually in intensity on the high-angle side. The peaks of (hk•0) lines are also displaced to the larger angles. These observations are explained by a theoretical analysis by Warren (1941) for two-dimensional diffraction. In our case, the single layer suspension naturally dried on glass plates seems similar to this kind of material. In Fig. 2.5(a), a line asymmetry is seen and a 3.5% displacement of (hk•0) lines relative to the original crystal toward larger angles is observed. These observations indicate that the sample investigated is random stacking single layers. The very broad (002) line and the absence of higher order (00•ℓ) lines indicate that the dimension of the parallel layer group perpendicular to the layers is very small, mostly a few layers thick. Thin films of about 1000Å thick obtained by repeated adding and drying suspensions up to 15 times did not give a sharp (002)

diffraction either (Fig. 2.5(b)). This fact suggests that the material consists of a distribution of groups of various small N of parallel layers, such as two, three, or four-parallel-layer groups, with approximately equal c spacing. Klug and Alexander (1954) express the scattering profile for a distribution of N-parallel-layer groups as

$$I = \sum_N \frac{P_N \sin^2\left(\frac{2\pi N d \sin\theta}{\lambda}\right)}{\sin^2\left(\frac{2\pi d \sin\theta}{\lambda}\right)} , \qquad (2.6\text{-}2)$$

where P_N is the percentage of each N, other symbols have the same meaning as in Eq. (2.6-1). By using this expression they fitted an observed (002) profile of a carbon sample measured by Franklin (1950) quite well by supposing that the sample is a mixture of two discrete sizes with 60% of the sample consisting of two-parallel-layer groups and 40% of five-parallel-layer groups. In our case for TaS_2 it is difficult to determine the percentage of each type of group because we do not have adequate profiles and part of the (002) line falls in the hole of the film. Nevertheless, from the broadness of the (002) line and a comparison of the width and shape of the (002) profile shown in Fig. 2.11, which is drawn for N = 2, we

can say that the sample consists mostly of two and three-parallel-layer groups. The estimated average value of the c spacing (~ 6.3Å) for the groups is slightly higher than the c spacing of TaS_2 crystals ($\Delta c/c_o \sim 4\%$). This is in agreement with Biscoe and Warren's (1942) result for carbon black, where they found that the c spacing of the two-dimensional carbon black is appreciably greater than the graphite value ($\Delta c/c_o \approx$ 2% - 6%). The reason is that in a random stacking situation each layer does not find the most suitable stacking position (corresponding to the lowest energy) and a larger c spacing results.

In the so-called random stacking single layer TaS_2 material some of the two or three-parallel-layer groups may be mutually oriented and provide weak, diffuse hk•ℓ ($\ell \neq 0$) reflections. But most of them are randomly stacked together. By contrast, the centrifuged deposits of single layer TaS_2 suspension are somewhat different. Here the layers form a large N of parallel layers with the same c spacing as indicated by the sharp (002) line in Fig. 2.5(c). The c spacing is the same as in 2H-TaS_2. It is thought that the relatively high pressure caused by centrifugation (~ 650g's) forces a large number of layers to orient parallel to one another While, when single layers are dried on glass, the uneven thickness of the dried layers (Fig. 2.6) and the severe drying conditions encountered by the single layers at the

glass-suspension interface prevent the formation of a large N of parallel layers.

In summary, the X-ray studies show that a highly disordered film is obtained by drying single layer suspensions on glass surfaces. The film appears to be made up of parallel layer groups of only a few layers thick (less than four layers). Such a model is shown schematically in Fig. 2.12, where each line represents a molecular layer and each set of parallel lines represents a parallel layer group. This highly disrupted structure likely results from the severe drying conditions encountered by the single layers at the glass-suspension interface. A photograph of a TaS_2 film dried on glass is shown in Fig. 2.6.

The structure of the dried, restacked layers is of interest because it is anticipated that there will be considerable interest in studies of the properties of such layers -- for example, the electrical conductivity, charge density wave formation and superconductivity of the ultra thin restacked layers. It is anticipated that further work will be done on such two-dimensional layers.

2.7 Summary

Freely floating single layers of TaS_2 and NbS_2 have been prepared using electrochemical and ultrasonic techniques. The so-called "electric shock" technique, i.e. sharp increase in

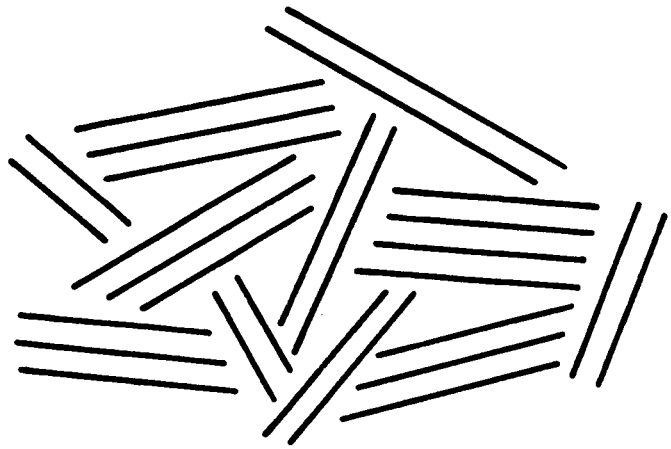

Fig. 2.12: Schematic model of random stacking single layer TaS_2. The layers are stacked randomly within a parallel layer group.

current in the end of electrolysis is found useful for uniformly separating the layers. A sequence of experiments has been carried out to confirm the single layer form. The major experiments and the relative figure numbers of the results for TaS_2 are shown schematically in a box-diagram (Fig. 2.13).

From the X-ray results we conclude that in the "soft" water-expanded crystals, water molecules have separated each layer for more than 100Å. This large separation reduces the interlayer coupling dramatically, as a result the "soft" water-expanded crystals can be suspended ultrasonically within a few seconds.

The two-dimensional character shown by the X-ray patterns of the "soft" water-expanded crystals and the dried random stacking single layers (Fig. 2.3(b) and Fig. 2.5(a)) give strong support to the freely floating single layer form of TaS_2 and NbS_2 in water suspensions.

It is believed that when these freely floating single layers restack on glass, most of them are randomly oriented in translation parallel to and rotation normal to the layers.

In contrast to the tremendous changes observed in the c axis, no noticeable change within one percent was observed for the a parameter in all the forms we studied for both TaS_2 and NbS_2. This shows that the intralayer bonding is very strong and disturbances like the intercalation of hydrogen and water,

Fig.2.13: Block diagram showing production of single layers and various forms of material studied.

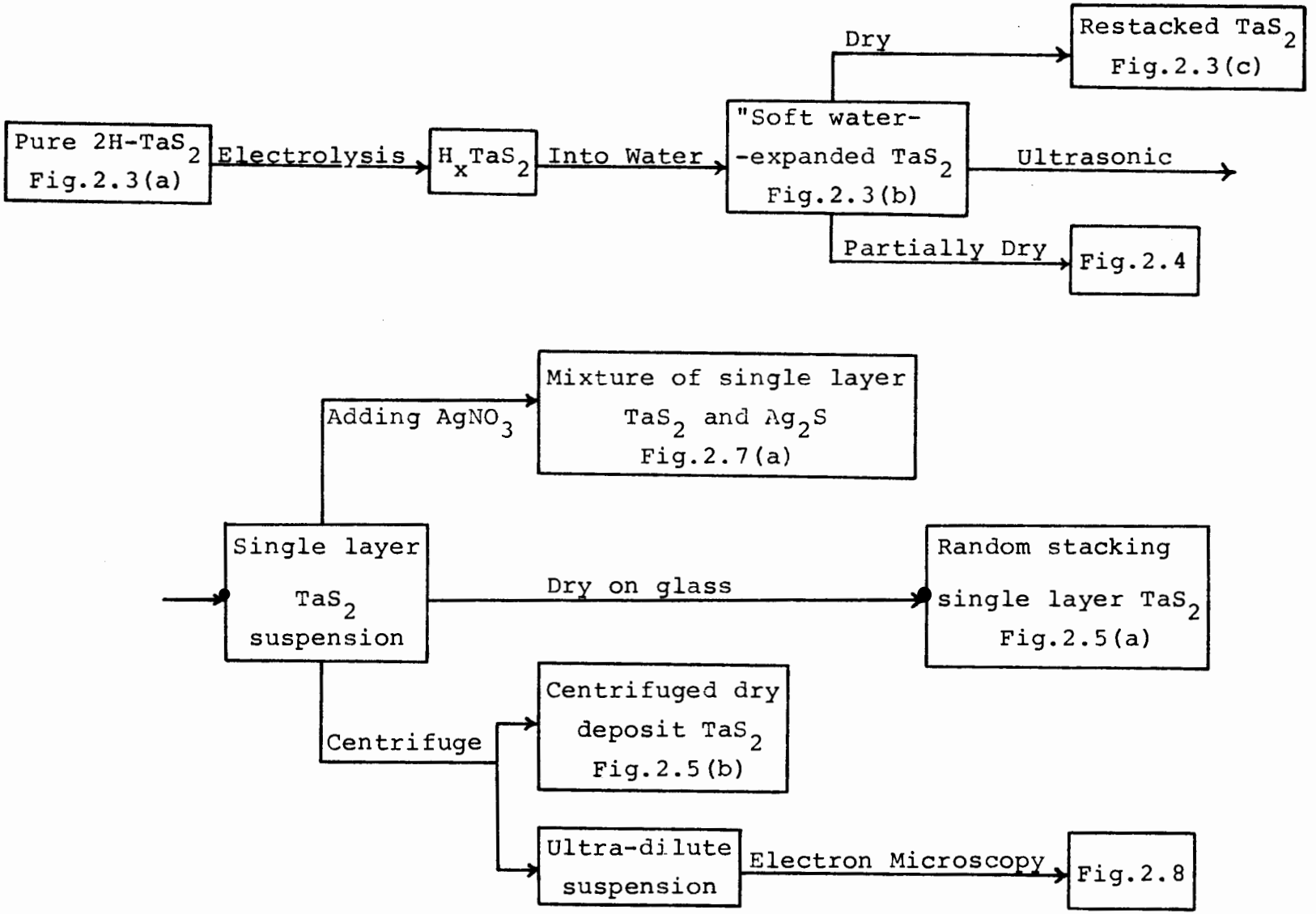
Pure 2H-TaS2
Fig.2.3(a)
Electrolysis
HxTaS2
Into Water
"Soft water-
-expanded TaS2
Fig.2.3(b)
Dry
Restacked TaS2
Fig.2.3(c)
Ultrasonic
Partially Dry
Fig.2.4
Adding AgNO3
Mixture of single layer
TaS2 and Ag2S
Fig.2.7(a)
Single layer
TaS2
suspension
Dry on glass
Random stacking
single layer TaS2
Fig.2.5(a)
Centrifuge
Centrifuged dry
deposit TaS2
Fig.2.5(b)
Ultra-dilute
suspension
Electron Microscopy
Fig.2.8

ultrasonic treatment, centrifugation and adding $AgNO_3$, etc., have no noticeable influence on the a parameter of the crystals.

Chapter 3

Optical Absorption Studies of Single Layers TaS_2 and NbS_2

3.1 Introduction

Optical absorption studies can provide useful information about the band structure and changes in the Fermi surface of the material studied. For a metal, absorption mainly results from interband excitation and the interaction between the incident electromagnetic wave and a very large concentration of free carriers (usually electrons) which are very polarizable and interacting readily with an incident e.m. wave (the so-called free-electron plasma resonance). Free carrier absorption is characterized by the plasma frequency ω_p, which has a simple expression

$$\omega_p = (4\pi ne^2/m^*)^{1/2} \qquad (3.1\text{-}1)$$

where n is the concentration and m^* the effective mass of free carriers.

Obviously, the free carrier absorption is proportional to the number of carriers per unit volume and also depends inversely on their effective mass, m^*. It can be shown (e.g. Wang, 1966) that the absorption coefficient α increases approximately as the square of the wavelength λ:

$$\alpha \propto \lambda^2 \qquad (3.1\text{-}2)$$

so that the free carrier absorption becomes more significant in the infra-red. The absorption coefficient α is defined, neglecting reflection losses, by

$$I = I_o e^{-\alpha t} \qquad (3.1\text{-}3)$$

where I_o is the intensity of incident light on the sample and I is that transmitted through the sample and t is the sample thickness.

The interband transitions for most metals usually occur in the ultra-violet wavelength region corresponding to a band gap of several electron volts. Combining these two processes we can see that the absorption spectrum of a metal is characterized by main peaks at several eV followed by a fall in absorption and rising again in the low energy region. The minimum in the spectrum reflects the degree of overlap of the interband and free carrier processes.

As introduced in Chapter 1, the optical properties of single crystals of the metallic layered compounds such as 2H-TaS_2 and 3R-NbS_2 have been extensively studied. About ten years ago, because of the interest in "two-dimensional" superconductivity there was a great deal of interest in organically intercalated layered metals (Gamble et al, 1970). This work led to an interest in the optical properties of the "two-dimensional" organic intercalation complexes of some of the Group IVB and VB layer compounds where a model of charge transfer from the organic molecules to the host materials is suggested to explain the changes in the spectra before and after intercalation (Beal and Liang, 1973). In addition, there has been an interest in the effects of thickness on the optical properties of the semiconducting layer compounds (Consadori and Frindt, 1970), where it is found that for MoS_2 and WSe_2 crystals less than about 100Å thick, a suppression of exciton absorption occurs. It is felt that isolated single layers are the closest possible physical realization of a two-dimensional system and thus the properties of such layers are of considerable interest, and particularly so in the light of the recent interest in localization effects (Thouless, 1977; Giordano, 1980).

The uniform suspensions of single layer TaS_2 and NbS_2 we obtained allowed us to study the optical absorption spectra of single layers in the region from 300 to 1200nm (6.2eV to

1.03eV). The lower energy region is limited by absorption from water, however, this limitation can be overcome by drying single layer suspension on a quartz plate.

3.2 Experimental

A double beam Cary 17 scanning spectrophotometer was used for some of the optical absorption measurements. These measurements were carried out for single layer TaS_2 and NbS_2 suspensions in water, for randomly stacked NbS_2 layers on quartz, for ultra-sonically obtained fine 2H-TaS_2 particles in suspension in water and for thinly cleaved 2H-TaS_2 and 2H-NbS_2 single crystals at room temperature in the atmosphere.

3.2.1 Optical Absorption of TaS_2 Single Layers, Particles and Single Crystals -- Sample Preparation

A TaS_2 single layer suspension in water was prepared as described in Section 2.1. A surfactant Triton X-705 (1% in volume) was added to a yellow-brown TaS_2 single layer suspension to prevent flocculation. A 10mm optical path quartz cell was used and another identical cell with water and 1% Triton X-705 was used as the reference.

For comparison, a pure single crystal and fine powder suspension of the original 2H-TaS_2 was also measured. A thin single crystal specimen of thickness 500-800Å (light yellow to orange-brown in transmission) was prepared by mounting a

crystal (about 3mm across) on a fused quartz disk with a small amount of epoxy and repeatedly peeling the crystal using sticky tape. To eliminate scattered and stray light the epoxy used was minimal and a dark paper shield with a 2mm diameter hole was used for both sample and reference disks.

A fine TaS_2 powder suspension was ultra-sonically prepared from the same batch of 2H-TaS_2 crystals. The 1% Triton X-705 surfactant was used in both sample and reference cell (10mm path length) and the measurement was carried out immediately after the suspension was prepared.

The Cary 17 spectrophotometer was operated in the range from 300nm to 1200nm (4.14 - 1.03eV) for the suspended samples and from 300nm to 1400nm (4.14 - 0.89eV) for the thinly cleaved sample, i.e. all the three regions (ultra-violet, visible and infra-red) were used.

Since our major concern was the shape of the absorption spectra, the sample thicknesses were not measured and the scattering due to unevenness in the thinly cleaved crystal samples was ignored.

The 2H-TaS_2 crystals used were all from growth batch "S".

3.2.2 Optical Absorption of NbS_2 Single Layers, Regrown Layers and Single Crystals -- Sample Preparation

The optical absorption of NbS_2 single layer suspensions has been somewhat extensively studied because of their

stability with regard to flocculation. Yellow-brown NbS_2 single layer suspensions were prepared as described earlier. A pair of 1mm optical path length quartz cells was used.

A random stacking NbS_2 thin film (regrown layers) of about 500Å thick was obtained by drying NbS_2 single layer suspensions on the surfce of a 1mm path length quartz cell. A single crystal sample of about 800Å thick for an optical measurement was prepared from the original 2H-NbS_2 crystals using the same method which was used for TaS_2.

A Cary 17 spectrophotmeter was used in the range 300-1200nm for NbS_2 single layer suspension and 300-1400nm for pure 2H-NbS_2 sample. For the random layer stacking NbS_2 sample the measurement was extended into the infra-red region to λ = 2500nm ($\sim$ 0.5eV). This wide spectrum range was limited for the sample in suspension due to the absorption of water and for the single crystal sample due to the wrinkled surface of the crystal and the stray light scattered from the non-uniform epoxy layer.

3.3 Experimental Results

3.3.1 Optical Absorption of TaS_2 Single Layers, Particles and Single Crystals

The room temperature Cary 17 spectrophotometer results for various forms of TaS_2 studied are shown in Fig. 3.1, where the spectra of TaS_2 single layer suspension in water (solid

Fig.3.1: Optical absorption spectra of a TaS_2 single layer suspension (——), thinly cleaved 2H-TaS_2 (----) and an ultrasonically prepared 2H-TaS_2 fine particle suspension (·····).

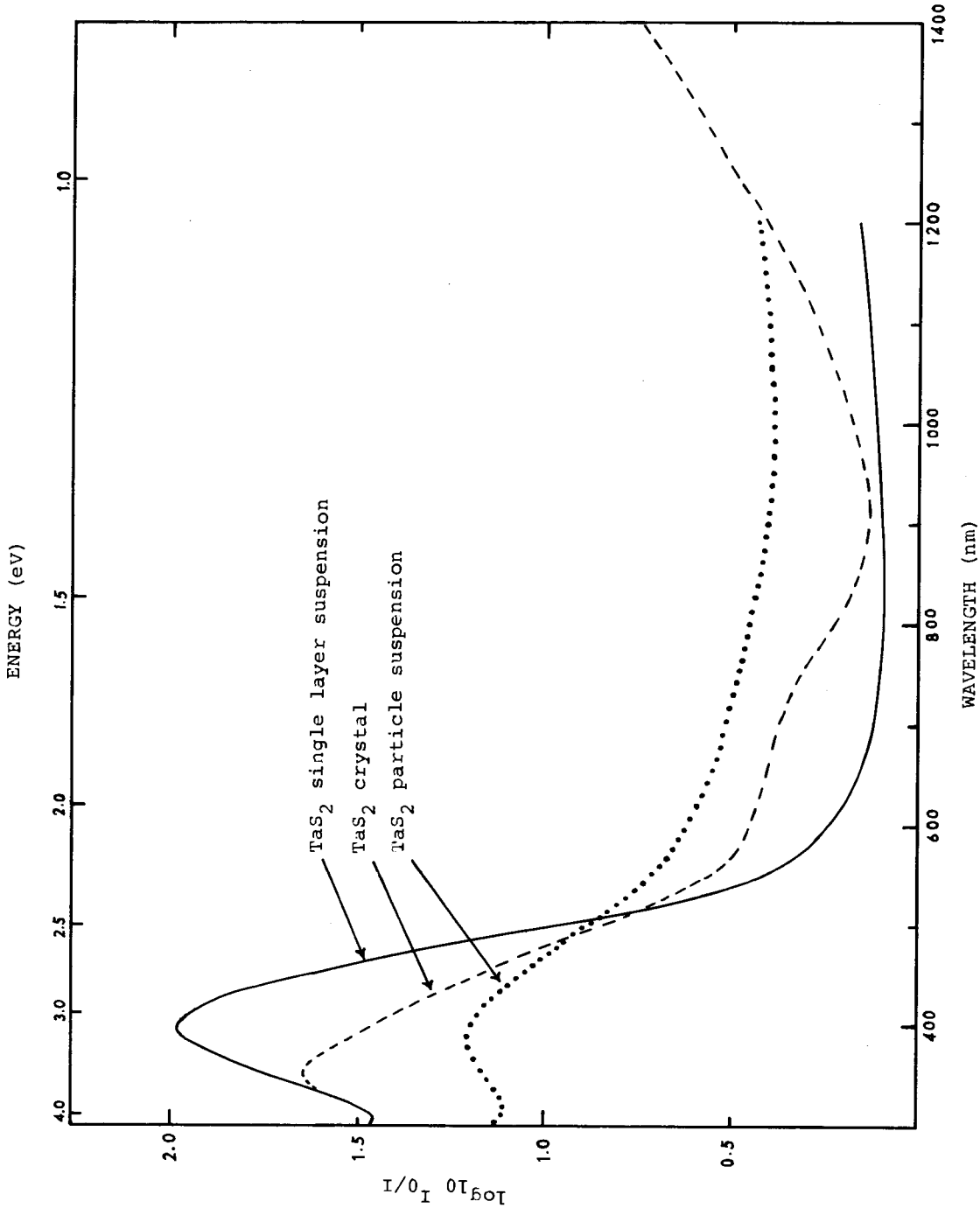
ENERGY (eV)
4.0
3.0
2.5
2.0
1.5
1.0
WAVELENGTH (nm)
400
600
800
1000
1200
1400
$\log_{10} I_0/I$
2.0
1.5
1.0
0.5
TaS_2 single layer suspension
TaS_2 crystal
TaS_2 particle suspension

line), a thinly cleaved 2H-TaS_2 (broken line) and an ultrasonically prepared 2H-TaS_2 fine powder suspension in water (dotted line)are given on the same diagram for easy comparison. Since the major concern is the shape and the absorption peak position, the vertical co-ordinate is left as the logarithm of I_O/I to the base 10, as given directly by the Cary 17 spectrophotometer.

The spectrum of a thinly cleaved 2H-TaS_2 crystal is similar to the results of Beal and Liang (1973) for 2H-TaS_2. The free carrier absorption edge starting around 1000nm (1.24eV) is easily seen. The main absorption peak is at 350nm ($\sim$3.55eV) and there is a shoulder around 600-700nm. The main peak, the absorption edge and the shoulder are in agreement with Beal and Liang's results. It is thought that the 700nm shoulder in the spectrum of thinly cleaved 2H-TaS_2 may be an inter-ference effect between the crystal surfaces. The absence of this shoulder in the spectra of suspension samples confirms this suggestion.

The spectrum of the TaS_2 single layer suspension is in close agreement with the results of Murphy and Hull (1975) for a similar TaS_2 dispersion. The main absorption peak is at 395nm and the free carrier absorption edge in the region of 1 to 1.5eV is almost completely absent.

The spectrum of 2H-TaS_2 dilute fine powder suspension is rather flat due to the non-uniformity and low concentration of

the suspension. In spite of this, it is of interest to note the similarity of this spectrum to that of the TaS_2 single layer suspension. The main absorption peak is at 390nm which is very close to the main peak of single layer suspension. The free carrier absorption edge is weakly evident and there is no shoulder around 600 to 700nm in both spectra.

3.3.2 Optical Absorption of NbS_2 Single Layers, Regrown Layers and Single Crystals

Fig. 3.2 shows the spectra of a dilute yellow-brown NbS_2 single layer suspension in a 1mm optical path length cell, a thinly cleaved 2H-NbS_2 crystal ($\sim$ 800Å thick) and a thin film ($\sim$ 500Å thick) of random stacking NbS_2 single layers on quartz. The major features of these spectra are similar to those for TaS_2. The main absorption peaks of the solid sample are at 430nm ($\sim$ 2.9eV), while for the single layer suspension the main peak is at 445 nm. The shoulder around 700-800nm which appears in the spectrum of the 2H-NbS_2 crystal is not seen in the spectrum of the single layer suspension and is very low in the spectrum of random stacking layers. The free carrier absorption edge which appears in the spectrum of 2H-NbS_2 around 1eV is not evident in both the random stacking and single layer suspension spectra. For the random stacking NbS_2 layers, the measurement was extended to 2500nm (0.496eV) and it was found that the absorption remained rather

Fig.3.2: Optical absorption spectra of NbS_2 single layer suspension (——), thinly cleaved 2H-NbS_2 crystal (- - - -) and thin film of random stacking NbS_2 layers on quartz (•••••).

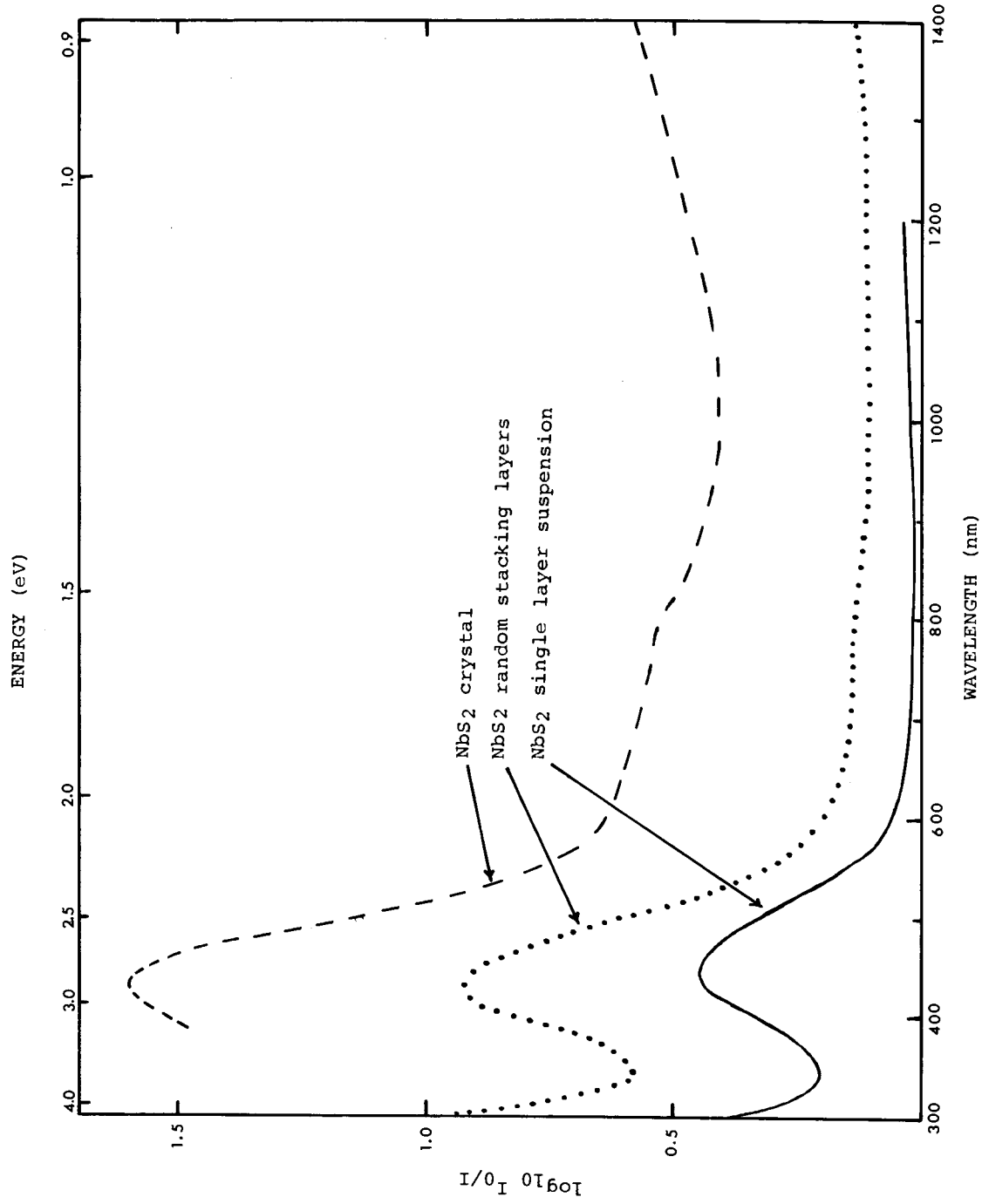
ENERGY (eV)
0.9
1.0
1.5
2.0
2.5
3.0
4.0
WAVELENGTH (nm)
1400
1200
1000
800
600
400
300
$\log_{10} I_0/I$
1.5
1.0
0.5
NbS_2 crystal
NbS_2 random stacking layers
NbS_2 single layer suspension

low. $Log_{10}\ I_O/I$ rises from a minimum value of 0.11 at 1000nm to 0.4 at 2500nm, while at the main peak $\log_{10}\ I_O/I$ =0.92. In terms of the absorption coefficient α, the ratio of α at 0.495 eV to α at the main peak is about 1/2.3, which is lower than Beal and Liang's (1973) results of ~1/1.2 for 3R-NbS_2. (the α ratio in our case neglects reflection.)

3.4 Discussion of Optical Absorption of Single Layer Suspension of TaS_2 and NbS_2

The optical absorption spectra of the single crystals as shown in Fig. 3.1 and Fig. 3.2 have been interpreted in terms of recent band models for the group V compounds (Fig. 1.4(b)). The main peak observed at 2.8eV is considered to arise from "d_{z2}" to "d/p" band transitions and some contribution may also come from the "p/d" to "d_{z2}" or even from "p/d" to "d/p" band transitions depending on the amount of "p/d" - "d_{z2}" overlap (Beal and Nulsen, 1981). The free carrier absorption in the spectra of thinly cleaved single crystals below 1eV is due to the high concentration of free electrons in the half-filled "d_{z2}" band. Any deviation from a half full band will result in reducing the effective number of free carriers (Beal and Nulsen, 1981).

As one can see from Fig. 3.1 and Fig. 3.2, the spectra of single layer suspensions and that of 3-dimensional samples as

a whole are quite similar with some differences below about 2eV. The general similarity in the curves is not too surprising since in his band structure calculations Mattheiss (1973) discussed layer-layer interaction very clearly and showed that the introduction of interlayer interaction has only a small effect on the shape and separation of the energy bands. In Fig. 3.1 the main absorption peak for both the single layer TaS_2 suspension and the 2H-TaS_2 powder suspension seems to have a red shift of 0.16eV relative to the peak position for thinly cleaved 2H-TaS_2. From Fig. 3.2 it can be seen that the main peak for single layer NbS_2 suspension has a red shift of about 0.1eV while the main peak for random stacking NbS_2 single layers, which are dry, has no change at all. We can offer no explanation for the shifts except to note that a shift is observed only when the samples are in water. Further work on oriented suspensions is desirable here.

The weak shoulder around 1.7eV for both 2H-TaS_2 and 2H-NbS_2 is not observed in the single layer spectra, although a very weak shoulder is present in the spectra of the TaS_2 crystallites in suspension and the random stacking NbS_2 sample. This shoulder has been attributed to screened excitons (Wilson and Yoffe, 1969), transitions to or from the half-filled d band (Beal et al., 1975) and more recently (Beal and Nulsen, 1981) to an interference effect. Our observations tend to support the views that the shoulder is an interference effect.

The major difference in the optical spectra of thinly cleaved single crystals and single layer crystals appears in the low energy range, i.e. in the free carrier absorption. Of particular significance is the result that for the random stacking NbS_2 single layers where the reflectivity should be similar to a cleaved solid, the difference in free carrier absorption is still remarkable. This change in free carrier absorption is very similar to the organic complex intercalated group V layer compounds where the red shift of the free carrier absorption is explained by charge transfer from the organic molecules to the host. This charge transfer reduces the effective number of carriers since the "d_{z2}" band is then more than half full. In our case, the process of possible charge transfer is not clear but it may be due to the possible presence of the originally intercalated hydrogen. A reduction in the carrier concentration could also be related to a loss in stoichiometry of the single layers during their preparation. Another possibility is that the breakdown of the 2H stacking sequence may give rise to a reduced carrier concentration, and also a possible increase in the effective mass (no band calculations are available for other NbS_2 stacking sequences). It is clear that more work is required here.

The observed absence of the charge density wave superlattice in the single layer TaS_2 is likely related to one or

more of the above situations, and again more work is required here.

Chapter 4

Optical Absorption Studies of NbS_2 Single Layer Suspensions in a Magnetic Field

4.1 Introduction

It was found that platelets of both TaS_2 and NbS_2 align in a magnetic field such that the layers are perpendicular to the magnetic field. This behaviour was observed by hanging a platelet of TaS_2 (NbS_2) single crystal in a magnetic field with the c axis of the crystal perpendicular to the suspending thin wire. The anisotropy in magnetic susceptibility is responsible for this behaviour. (I thank Dr. A.S. Arrott for discussions on this.)

It is well known that a magnetic dipole of moment $\vec{\mu}$ in a uniform magnetic field $\vec{B}$ is subjected to a torque $\vec{L}$, given by

$$\vec{L} = \vec{\mu} \times \vec{B} \qquad (4.1\text{-}1)$$

so that the field tends to rotate the dipoles until they are parallel to the field.

For an isotropic diamagnetic or paramagnetic platelet in a magnetic field the induced dipole moments have no preferred crystal direction and the stable position of the platelet

would be that for the platelet aligned parallel to the field, as shown in Fig. 4.1. This is due to the difference between the demagnetization energy along the platelet and that perpendicular to the platelet. The situation is similar to a long diamagnetic or paramagnetic bar in a magnetic field, which has been studied thoroughly by Bozorth and Chapin (1942).

For an anisotropic crystal, however, the situation is different. An anisotropy in magnetic susceptibility χ causes the induced dipole moments to prefer the greater χ direction, and as a result the crystal in a magnetic field tends to align with the greater χ direction parallel to $\vec{B}$.

It was found that 2H-TaS_2 has an anisotropy in susceptibility with the ratio $\chi_\perp/\chi_\parallel$ around 2.2-2.5 (Hillenius and Coleman, 1978), where $\chi_\perp$ and $\chi_\parallel$ are the susceptibilities with $\vec{B}$ perpendicular and parallel to the crystal layers respectively. Thus it is clear that an anisotropic susceptibility is responsible for the fact that TaS_2 platelets tend to align in a magnetic field with the layers perpendicular to $\vec{B}$. A similar situation clearly applies for NbS_2 platelets.

MoS_2, however, is almost isotropic in susceptibility (Belougne and Zanchetta, 1972) and as a result, thin platelets of MoS_2 tend to align in a magnetic field with the layers parallel to $\vec{B}$. This behaviour was also observed by suspending

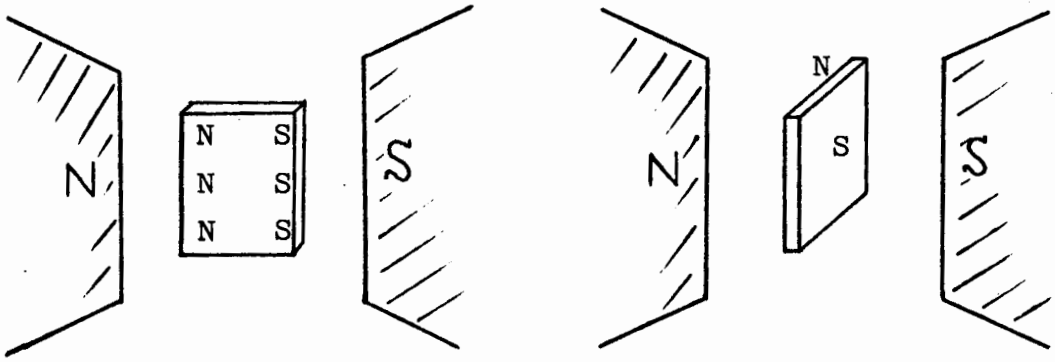

(a) Stable

(b) Unstable

Fig.4.1: Stable and unstable positions of an isotropic dia- or paramagnetic platelet in a magnetic field.

a thin platelet of 2H-MoS_2 single crystal in a magnetic field with the c axis of the crystal perpendicular to the suspending wire.

Because of the behaviour of TaS_2 and NbS_2 single crystal platelets in magnetic fields, we expect the same effect of magnetic field on single layer TaS_2 and NbS_2 suspensions.

Fig. 4.2 shows the effect of the magnetic field on a TaS_2 single layer suspension, where Fig. 4.2(a) shows the dark brown TaS_2 single layer suspension when B = 0 and Fig. 4.2(b) shows the same suspension becoming light yellow-brown in a field of 8 K Gauss. The same phenomenon was observed for NbS_2 single layer suspensions. The forces tending to align the crystal platelets are balanced by the thermal motion. When a dilute yellow-brown NbS_2 suspension and a higher field (23 K Gauss) was used, the suspension appeared just a very light yellow color, indicating that the alignment of single layers was more perfect. This alignment effect allows us to obtain optical information with the electric vector of the incident light nearly parallel to the c axis of the layers ($\vec{E} \parallel \vec{c}$) by using polarized light and magnetic field. This information is difficult to obtain for bulk layered crystals unless optically suitable crystal edges are available.

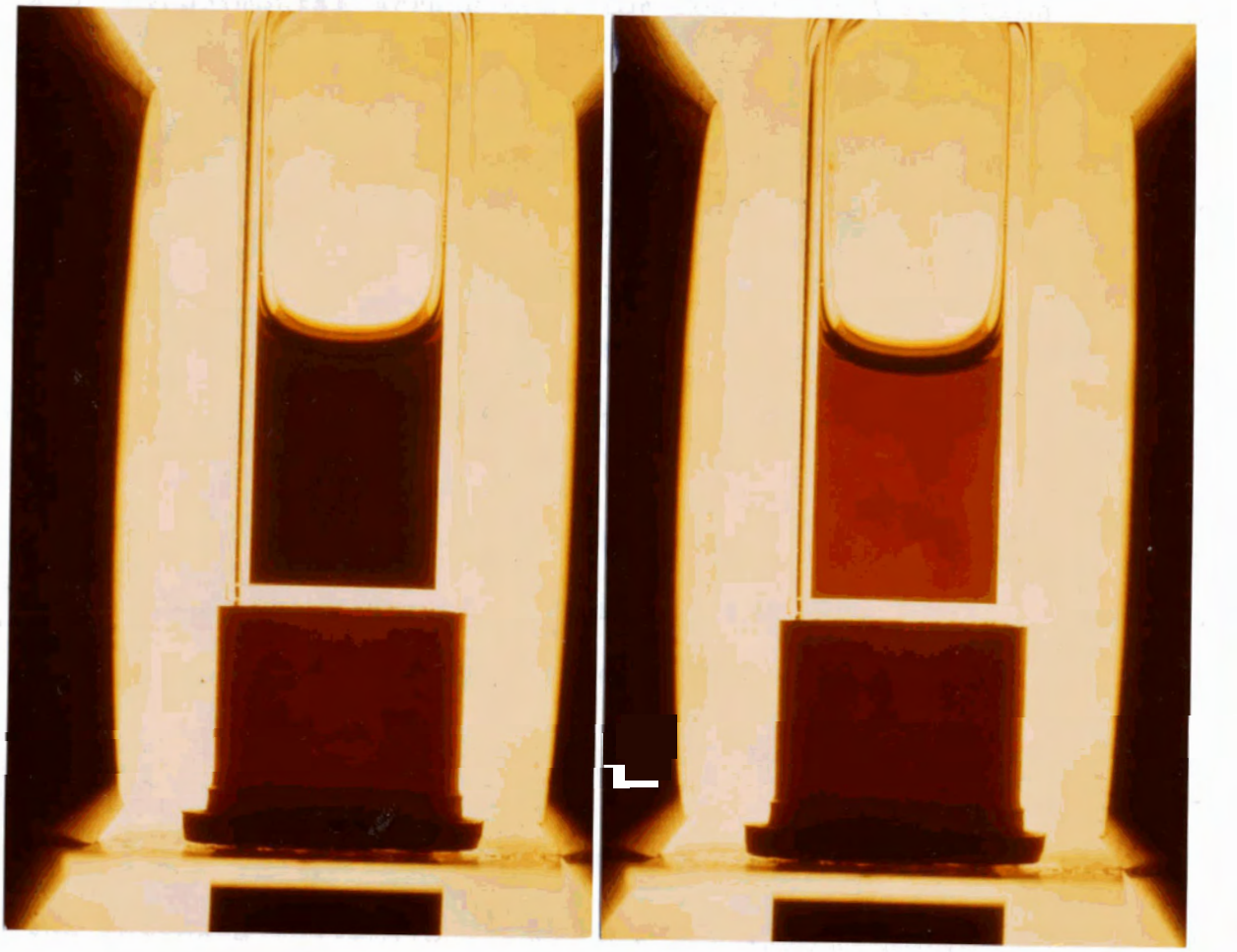

(a) (b)

Fig.4.2: Effect of a magnetic field on a dark brown TaS_2 single layer suspension

(a) B=0

(b) B=8 KGauss

(no polarizers).

4.2 Experimental Arrangement for Measuring Absorption Spectra of Single Layers in Magnetic Fields

To measure the absorption spectra of single layer NbS_2 suspensions with the electric vector of the incident light nearly parallel to the c axis of the crystal ($\vec{E} \parallel \vec{c}$) a magnet is needed to align the single crystals. This makes typical commercial spectrophotometers like the Cary 17 unsuitable for our special purpose and thus an experimental arrangement was assembled and the setup of the experiments is shown schematically in Fig. 4.3. Compared to the standard double beam technique, the present setup is characterized by the using of a Polaroid filter, a depolarizer and an electromagnet. The Polaroid filter was fixed on a vertically rotatable frame and careful adjustment was made to ensure that the Polaroid filter remains in the same vertical plane when it is rotated. Thus the incoming white light can be plane polarized in any direction in the vertical plane by rotating the Polaroid filter without changing the intensities of the outgoing polarized light beams. A small electromagnet was used and two pieces of iron plate of 4cm diameter were inserted into the magnet gap, reducing the gap to about 4.5mm so that the maximum magnetic field was 23 K Gauss. For the small magnet gap, a pair of special quartz optical cells with a 10mm optical path length and an inner thickness of 1.0mm were used as the sample and reference cells. They were fixed one over the other in

Fig.4.3: Set-up for optical absorption measurements of NbS_2 single layer suspension in a magnetic field. (a reference cell is positioned beside the sample cell)

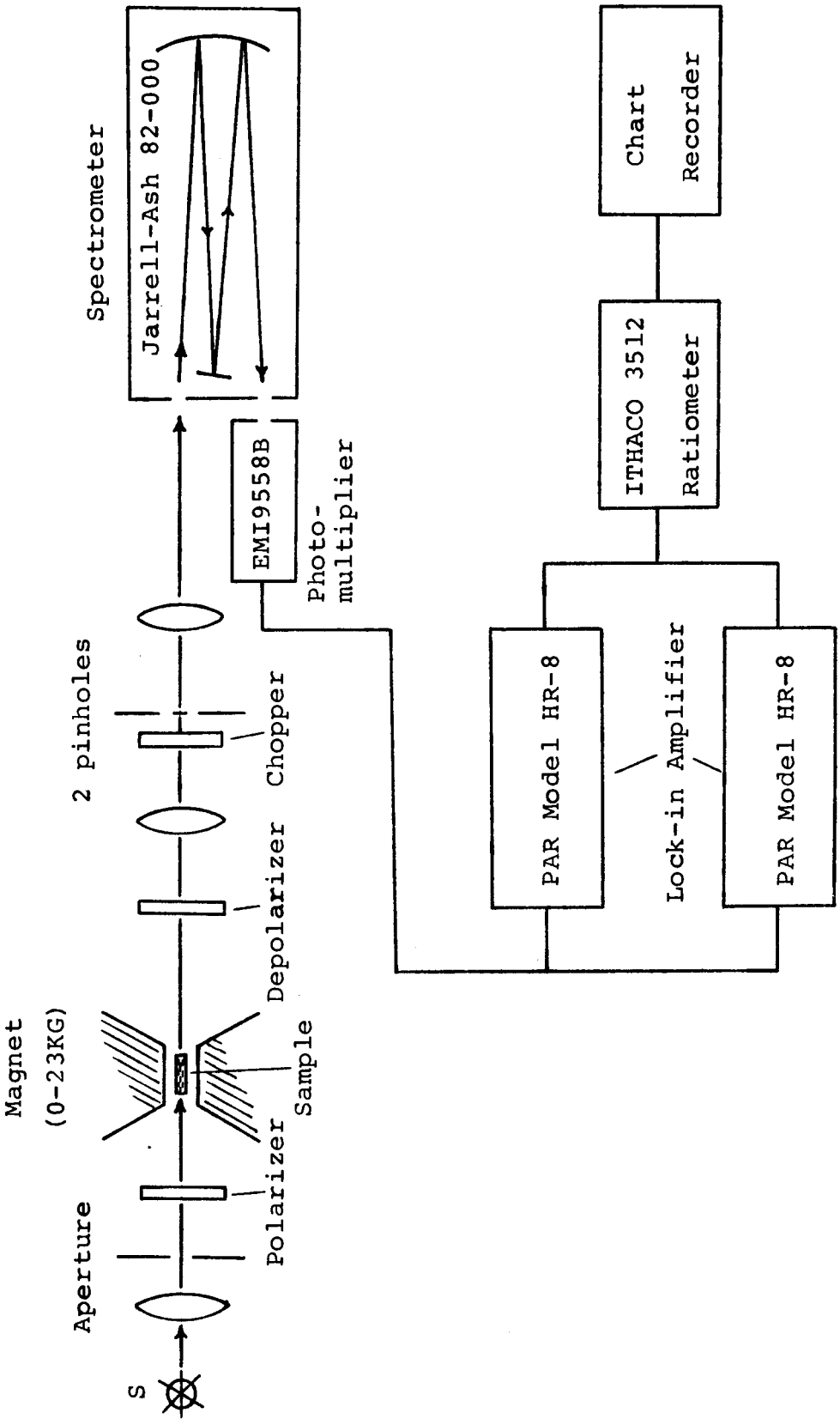
S
Aperture
Polarizer
Magnet
(0-23KG)
Sample
Depolarizer
2 pinholes
Chopper
Spectrometer
Jarrell-Ash 82-000
EMI9558B
Photo-
multiplier
PAR Model HR-8
Lock-in Amplifier
PAR Model HR-8
ITHACO 3512
Ratiometer
Chart
Recorder

the same vertical plane in the horizontal magnetic field. The incident parallel light beam was perpendicular to the direction of the magnetic field, that is, $\vec{k} \perp \vec{B}$, where $\vec{k}$ is the wave vector of the incident light. The images of the sample and the reference were focussed onto a two-frequency (40 Hz and 100 Hz) mechanical light chopper and a two-aperture screen. The light passing through the sample and the light passing through the reference were thus modulated by two different frequencies and two equal cross-sections of these light beams were selected by the two-aperture screen. Since the cells are rather narrow, a suitable composition of lenses was chosen and careful adjustment was made to ensure that the images of the sample and the reference cells were slightly larger than the apertures. The sample and reference beam were focussed onto the entrance slit of a Jarrell-Ash 82-000 spectrometer and the dispersed beams then entered a EMI 9558B photomultiplier. This tube has a S-20 response with the sensitivity peak at ~4200Å and allows a photon energy range from 1.8 to 3eV (λ from 4000Å to 7000Å) to be suitably investigated. Since the sensitivity of the photomultiplier is position dependent, the sample and the reference beam should be carefully adjusted so that the corresponding dispersal beams can be as close as possible on the photocathode. To eliminate the influence of magnetic field on the photomultiplier, the photomultiplier is shielded by mu-metal

sheets. The modulated sample and reference signals are picked up and amplified by a pair of PAR Model HR-8 lock-in amplifiers, and the ratio I_o/I is taken by an ITHACO 3512 ratiometer and recorded on a chart recorder.

To investigate the influence of magnetic fields on the absorption peak height, an X-Y recorder was used instead of the chart recorder and a Bell 620 gaussmeter was used to measure the magnetic field.

Since the spectrometer optics treat the different modes of polarization differently, a depolarizer was used in this experiment. The depolarizer used consists of two wedges of quartz (positive uniaxial crystal). The depolarizer was oriented with the wedge edge at 45° to the horizontal direction, thus we have the effect of a variable wave plate which produces effective depolarization for all wavelengths.

4.3 Measurements of the Optical Absorption Spectra of NbS_2 Single Layer Suspensions in Magnetic Field

The measurements were made for NbS_2 only, since NbS_2 single layer suspensions are much more stable than TaS_2 single layer suspensions with regard to flocculation. Dilute yellow-brown NbS_2 single layer suspensions in water were prepared as before. A pair of flat 10mm optical path length quartz cells were used, one for the sample and one filled with

water as a reference (for both sample and reference cells filled with water, the absorption spectrum was very close to a straight line in the desired range from 4000 to 7000Å). The reading of the wavelength in the spectrometer was calibrated using a mercury lamp.

Measurements were carried out first for B = 0. In the zero field and horizontally polarized incident light ($\vec{E} \parallel \vec{B}$), the spectrum of a dilute yellow-brown single layer NbS_2 suspension was measured in the range from 4000Å to 7000Å ($\sim 3.1 - 1.77$eV). It was found that when B = 0, the direction of polarization of incident light made no significant difference to the spectrum.

Then a magnetic field of 23 K Gauss was applied and the spectrum was measured with the sample and Polaroid filter unchanged. Finally, by rotating the Polaroid filter by 90°, the direction of polarization was changed from horizontal ($\vec{E} \parallel \vec{B}$) to vertical ($\vec{E} \perp \vec{B}$) and the spectrum of the same sample in a 23 K Gauss magnetic field and under vertically polarized incident light was measured.

During the measurement, since the sensitivity of the photomultiplier changes with wavelength, the sensitivity range of two lock-in amplifiers were adjusted to keep the amplifiers from overloading.

Attempts to solidify the aligned layers in suspension using gelatin and by cooling in a magnetic field were tried

without success. When the gelatin set, no optical anisotropy was observed, and when the suspension was frozen, it became opaque and no optical measurement could be made.

To investigate the influence of magnetic field on the absorption peak (at around 4600Å), the scanning spectrometer was fixed at 4600Å and an X-Y recorder was used. A Bell 620 gaussmeter was used with its probe fixed beside the sample cell. The magnetic field was varied slowly (from 0 to 23 K Gauss in about 5 minutes) to ensure that the single layers in suspension had enough time to align up. (When the magnetic field was changed it took just a few seconds for the layers to reach equilibrium.) The measurements were carried out for both B increasing and B decreasing and repeated several times. The consistency of results was quite good.

4.4 Experimental Results of Optical Absorption Measurements on NbS_2 Single Layer Suspensions in a Magnetic Field

Figure 4.4 shows the absorption spectrum of the single layer NbS_2 suspension in a magnetic field of 23 KG for $\vec{E}//\vec{B}$ and $\vec{E}\perp\vec{B}$, along with the spectrum of the same NbS_2 single layer suspension in zero field for $\vec{E}//\vec{B}$. When B=0, the spectrum is essentially the same as that obtained with the Cary 17 spectrophotometer except the main peak is now at 455 nm instead of 445 nm. When B=23 KGauss, a remarkable feature is the tremendous difference in absorption peak height for $\vec{E}//\vec{B}$ and $\vec{E}\perp\vec{B}$. The main peak height for $\vec{E}\perp\vec{B}$ is about 9 times that for $\vec{E}//\vec{B}$, while the main peak height for B=0 is exactly in between. Since the layers of NbS_2 are nearly aligned perpendicular to $\vec{B}$, it is reasonable to say that the main peak height(I_0/I at λ=4600A) for $\vec{E}\perp\vec{c}$ is 9 times that for $\vec{E}//\vec{c}$. To express the absorption peak in terms of the absorption coefficient α, we can assume that α is the same for the case of $\vec{E}\perp\vec{c}, \vec{k}\perp\vec{c}$ and for that of $\vec{E}\perp\vec{c}, \vec{k}//\vec{c}$ and assume in our experiment the "effective thickness" of the sample is the same for both $\vec{E}\perp\vec{c}, \vec{k}\perp\vec{c}$ and $\vec{E}//\vec{c}, \vec{k}\perp\vec{c}$. Using a value of α of 6.5×10^5 cm^{-1} at the main absorption peak for $\vec{E}\perp\vec{c}, \vec{k}//\vec{c}$ (Yoffe, 1974), we can estimate that the sample effective thickness is about 450A. This gives an α of about $1.6\times10^5 cm^{-1}$ for $\vec{E}//\vec{c}$ at the main peak. That is, the absorption

Fig.4.4: Optical absorption spectra of a NbS_2 single layer suspension in 23 KGauss magnetic field for $\vec{E}//\vec{B}$ (dotted line) and $\vec{E}\perp\vec{B}$ (broken line), compared with the zero field spectrum for $\vec{E}//\vec{B}$ (solid line).

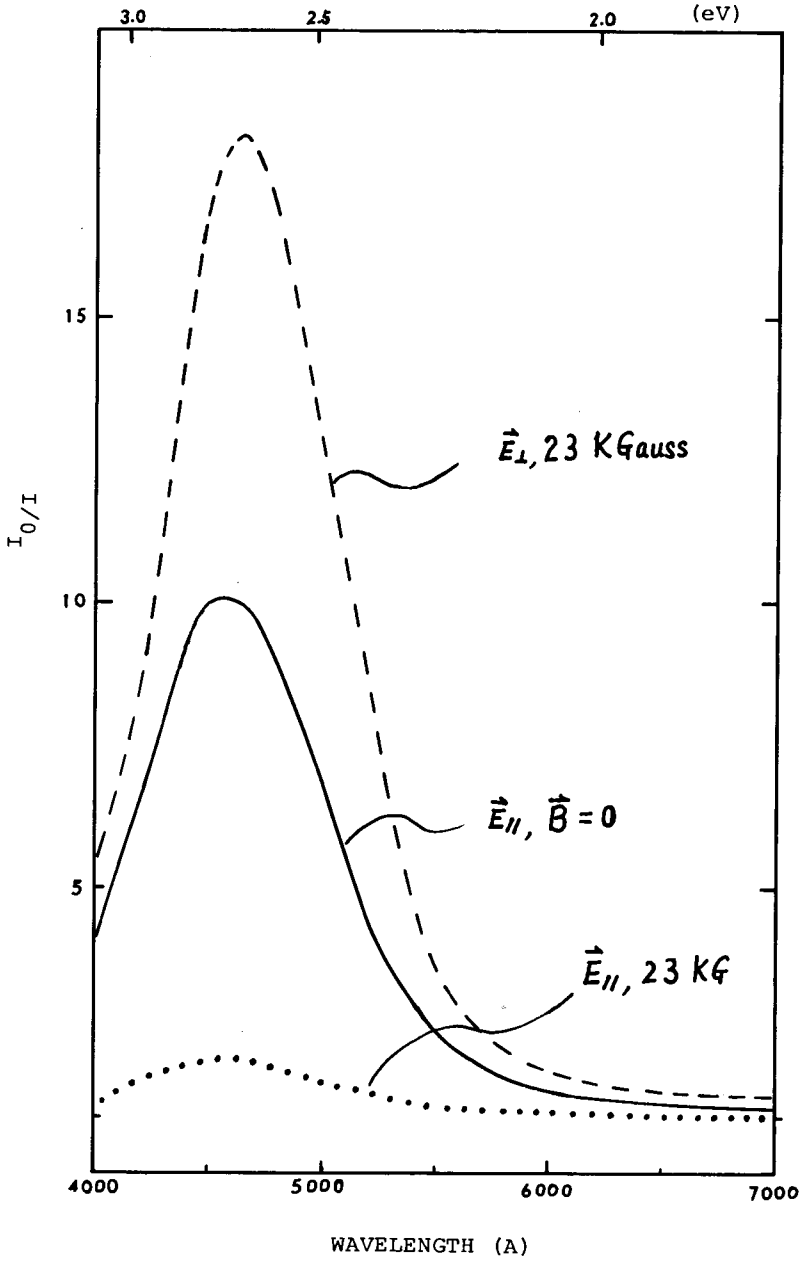
3.0
2.5
2.0
(eV)
15
10
5
$I_{0/I}$
$\vec{E}_{\perp}$, 23 KGauss
$\vec{E}_{//}$, $\vec{B}$ = 0
$\vec{E}_{//}$, 23 KG
4000
5000
6000
7000
WAVELENGTH (A)

constant at 2.7 eV for $\vec{E}\perp\vec{c}$ is about four times greater than that for $\vec{E}\parallel\vec{c}$.

It was also noticed that the main peak shifted from the zero field value of 4550Å to 4650Å (an energy shift of about 0.06 eV) when vertically polarized light ($\vec{E}\perp\vec{B}$) and 23 KGauss field were used. For $\vec{E}\parallel\vec{B}$, the main peak remained at 4550Å in the 23 KGauss field. It is of interest to note that with $\vec{E}\parallel\vec{B}$ polarized incident light, for $\lambda>6500$Å, the NbS_2 single layer suspension in the 23 KGauss field has no observable absorption ($I_o/I=1$).

Figure 4.5 shows the relation of the absorption peak height (I_o/I at $\lambda=4600$A) VS. magnetic field for both $\vec{E}\parallel\vec{B}$ and $\vec{E}\perp\vec{B}$. For $\vec{E}\parallel\vec{B}$, the absorption decreases rather fast as the magnetic field increases from 0 to 12 KGauss and then decreases more gradually with increasing B. For $\vec{E}\perp\vec{B}$, the absorption increases as the field increases, again tending to level off at high fields.

Fig. 4.5: Absorption peak height (I_0/I at λ=4600Å) VS. magnetic field for both $\vec{E}//\vec{B}$ (····) and $\vec{E}\perp\vec{B}$ polarized incident light (- - - -).

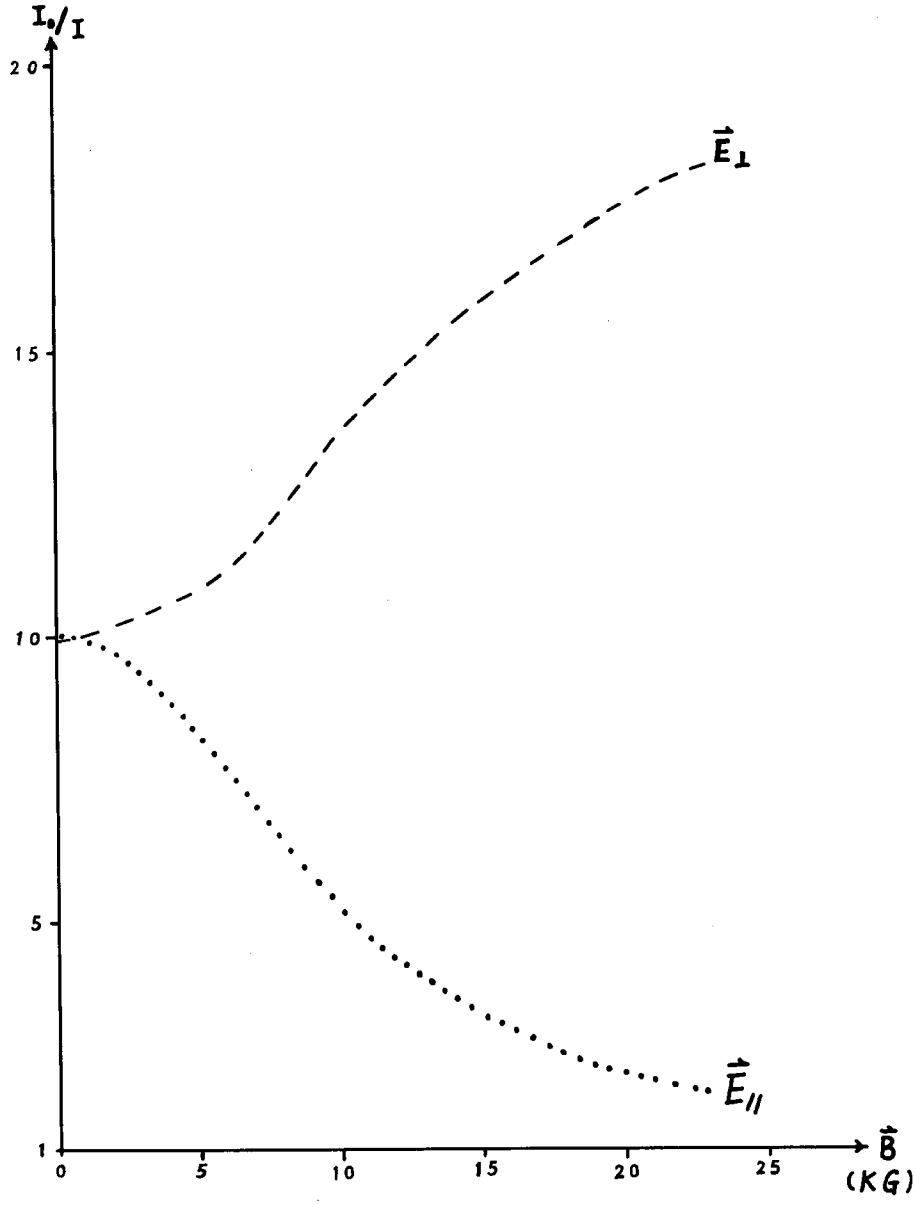
I_0/I
20
15
10
5
1
0
5
10
15
20
25
$\vec{E}_\perp$
$\vec{E}_{//}$
$\vec{B}$
(KG)

4.5 Discussion of Polarization Dependent Optical Absorption of NbS_2 Single Layer Suspensions

From Fig.4.5 it can be seen that when the magnetic field increases to high values (>23 KG), the absorption peak height (I_o/I at λ=4600Å) for both $\vec{E}//\vec{B}$ and $\vec{E}\perp\vec{B}$ polarized incident light tends to approach saturation. Thus in a sufficiently strong magnetic field the single layers of NbS_2 in suspension align themselves with the c axis nearly parallel to the field and the wave vector $\vec{k}$ of the incident light closely parallel to the layer plane (i.e. approximately $\vec{c}//\vec{B}$ and $\vec{k}\perp\vec{c}$). The situation can be shown schematically in Fig.4.6. Based on these considerations we can regard our experiments in the 23 KG field as an optical anisotropy study on single layer NbS_2. The tremendous difference in the optical absorption peak height for $\vec{E}//\vec{c}$ and $\vec{E}\perp\vec{c}$ can in principle be discussed in terms of the bulk anisotropic crystal structure and the selection rules which govern the interband transitions, to the extent that the multilayer models apply to single layers.

Liang (1973) has given a general discussion on the optical anisotropy of layered compounds and points out that a single layer having the trigonal prism coordination (such as a NbS_2 layer) is invariant under a reflective operation with respect to reflection in the Nb plane. The electric vector of the incident light, and hence the electric dipole operator, also transforms either with even or odd parity depending on $\vec{E}\perp\vec{c}$ or $\vec{E}//\vec{c}$ respectively. Since the transition

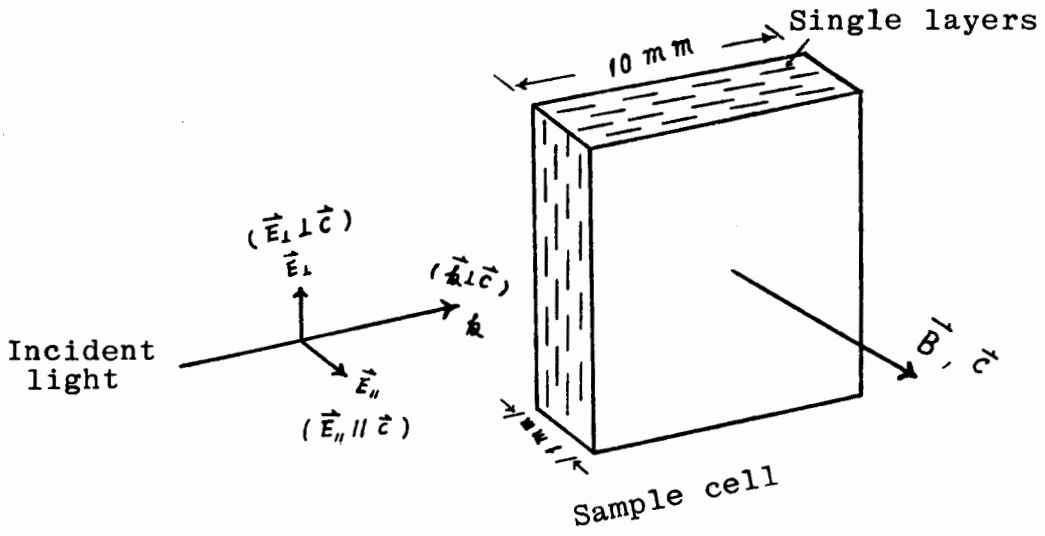

Fig.4.6: Schematic diagram showing the alignment of single layer NbS_2 (represented by short lines) in a magnetic field. The directions of the incident light, the magnetic field and the c axis of the single layers are also shown.

matrix element is made up from the product of wavefunctions of the initial and final states and the electric dipole operator (spin neglected), and is non-zero only when the product is an even function, only transitions between states of the same reflection parity contribute to the absorption for $\vec{E}\perp\vec{c}$ and only transitions between states of opposite reflection parity contribute the absorption for $\vec{E}\parallel\vec{c}$.

To connect our spectra for NbS_2 with band structure calculations, we note that transitions between high density of states regions are responsible for the absorption peaks in the optical spectra. Thus in an assignment of an observed transition peak to a band model, one generally looks for corresponding energies between flat band regions in the band structure.

Band structures of 2H-$NbSe_2$ have been calculated by Mattheiss (1973) and by Wexler and Woolley (1976), however, for 2H-NbS_2 only the lowest d sub-band is provided (Wexler and Woolley, 1976). An early and seldom cited calculation by Kasowski (1973) for 2H-MoS_2 and 2H-NbS_2 does exist, but it does not fit the NbS_2 results and it is also quite different from other calculations for 2H-MoS_2 and 2H-$NbSe_2$ and has been criticized by Mattheiss (1973).

The interband transition for single crystal 2H-NbS_2 at 2.7 eV has been discussed by Parkin and Beal (1980) and is attributed to "d_z2" to "d/p" transitions with a small contribution from "p/d" to "d/p" transitions (see the energy band scheme, Fig. 1.4). The nomenclature such as "p/d" indicates band hybridization — i.e., that the chalcogen "p" bands are hybridized with the metal "d" bands. Since pure "d" to "d" transitions are forbidden by selection rules, it is this hybridization that allows for the interband absorption between "d" bands. This assignment is consistent with the joint density of states calculations for 2H-$NbSe_2$ of Liang and Beal (1976) and Doran et al (1981). Both of these calculations ignore polarization effects.

A proper and significant comparison of our polarization results on single layer NbS_2 requires joint density of states calculations on a single layer model for interband transitions, with the inclusion of polarization effects.

In spite of a lack of theory appropriate to our results on single layer NbS_2, we can make some use of the single layer band model for MoS_2, recognizing that the band structure of single layer NbS_2 is expected to be similar to that for MoS_2 (Mattheiss, 1973). The interband peak at 2.7 eV for 2H-NbS_2 is also observed in 2H-MoS_2 at 2.8 eV. We use the transition

assignments made for MoS_2 for a single layer model by Beal et al (1972) to help analyse our results.

The two dimensional Brillouin zone (Bromley et al, 1972) and Beal et al's experimentally fitted band structure of single layer MoS_2 are shown in Fig. 4.7(a) and Fig. 4.7(b) respectively. In Fig.4.7(b) the bands of odd and even parity with respect to the reflection on the plane of the layer are represented by broken and solid lines respectively. From Fig.4.7(b) it can be seen that the energy gap between Q_2^- in the top valence band and Q_2^- in the conduction band is 2.76 eV. Beal et al's (1972) assignment states that $Q_2^- \longrightarrow Q_2^-$ corresponds to the 2.76 eV absorption peak in the spectrum of 2H-MoS_2. This transition is very close to the 2.7 eV observed in the spectrum of NbS_2. Other gaps deviate even further. Thus the absorption peak at 2.7 eV for NbS_2 may be due to the transitions between two flat bands at Q_2^- (in the top valence band) and Q_2^- (in the conduction band), i.e., $Q_2^- \longrightarrow Q_2^-$. This transition is allowed for $\vec{E} \perp \vec{c}$ only since it is between states of the same reflection parity.

The results reported here are the first optical anisotropy studies made on the layered compounds using absorption measurements. Since strong absorption is accompanied by high reflectivity, it is of interest to compare our measurements with measurements on the anisotropic reflectivity from the edge of layered compounds made by Liang (1973). No observa-

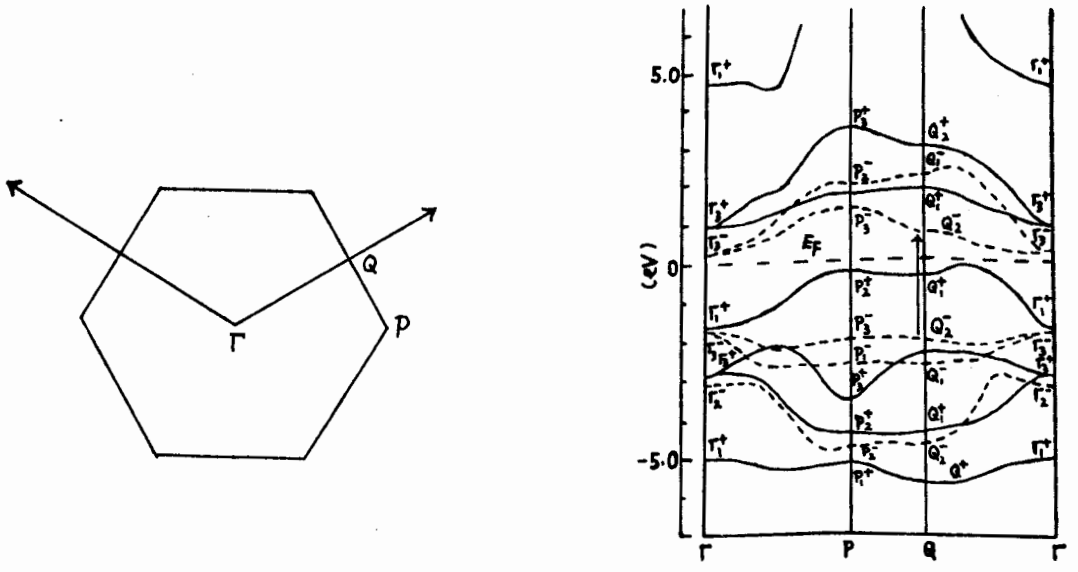

(a) (b)

Fig.4.7: (a) The two dimensional Brillouin zone of MoS_2

(b) Experimentally fitted single layer band structure of MoS_2, where bands of odd and even parity with respect to the reflection on the plane of the layer are represented by broken and solid lines respectively.

((a): taken from Bromley et al, 1972

(b): taken from Beal et al, 1972)

tions have been made for 2H-NbS_2 for $\vec{E}//\vec{c}$, however, Liang has measured the edge reflectivity spectra of 2H-$NbSe_2$ and 3R-NbS_2 at 78°K for both $\vec{E}\perp\vec{c}$ and $\vec{E}//\vec{c}$. For 2H-$NbSe_2$ a weakened reflectivity peak at 2.5 eV is observed for $\vec{E}//\vec{c}$ relative to $\vec{E}\perp\vec{c}$. In contrast, for 3R-NbS_2 the reflectivity peak observed at 2.7 eV is strongly suppressed for $\vec{E}//\vec{c}$. The photon energy range in Liang's reflectivity spectra is too narrow to make a Kramers - Kronig analysis and as a result it is impossible to make a quantitative comparison with our results, however, it is safe to say that the reflectivity results in both cases are consistent with our absorption results and in particular the transition at 2.7 eV appears to be strongly suppressed for $\vec{E}//\vec{c}$ in 3R-NbS_2. The degree of suppression of the transitions for both the 3R-NbS_2 and the single layer NbS_2 results gives some support to the view that the 3R structure is more "two-dimensional" than the 2H structure (Beal et al, 1972). In the 2H structure the Nb stacking is AAA···, whereas in the 3R structure the Nb stacking is ABC ABC ···. There thus appears to be more interaction between the layers when the Nb atoms are stacked directly above one another, as is the case for the 2H structure.

It would be desirable to extend our measurement to both

higher and lower energies so that other features of the spectrum can be observed. At present this extension is limited by our instrumentation, nevertheless the observed anisotropy in the interband transition for $\vec{E} \perp \vec{c}$ and $\vec{E} \parallel \vec{c}$ is remarkable and the technique of aligning small crystal platelets (not necessarily single layers) in suspension in a magnetic field will be useful in the optical anisotropy studies of many layered compounds.

Chapter 5

Conclusions

A method of electrointercalation of hydrogen and water into single crystal of 2H-TaS_2 and 2H-NbS_2 followed by ultrasonic dispersion has been successfully used to make TaS_2 and NbS_2 single layers in suspension. The X-ray diffraction results have convincingly shown the various single layer forms. It was found that each layer was separated by water for at least 100Å in the "soft", water-expended TaS_2 and NbS_2. The deintercalation of water was observed within about an hour. In order to get freely floating single layer suspensions, the ultrasonic dispersion must be carried out as soon as the crystals are water-expanded.

On the basis of observations on single layers and the restacked layers, it was concluded that the layers retain the same structure as the original bulk crystals with the a parameter remaining unchanged to within one percent. Single layers were examined under the electron microscope and no charge density wave superlattice was observed down to 25°K. It is believed that when the single layers restack on glass most of them are randomly oriented and thin films formed in this way appear to be made up of parallel layer groups, each of them only a few layers thick. These thin films are believed to be more "two-dimensional" than the bulk layered material and would be suitable for studies of two-dimensional

electrical conductivity, superconductivity, Raman scattering and charge density wave formation etc.

The optical absorption studies for various forms of single layers over the photon energy range from 0.9 to 4.0 eV showed no significant change in the interband excitation compared to the bulk material. The apparent suppression in free carrier absorption is likely due to a reduction in the number of free carriers but the reason for this reduction is open to speculation. The general similarity in the interband transitions between the single layer suspensions and the original bulk material is not surprising since the interlayer coupling has only a small effect on the band structure (Mattheiss, 1973). On the other hand, one might expect some differences in the absorption of the suspensions due to the fact that all crystallite orientations are presented to the beam.

The single layers of TaS_2 and NbS_2 in suspension can be aligned in a sufficiently high magnetic field with $\vec{c} // \vec{B}$. From the polarization dependent optical absorption measurements for NbS_2 single layer suspensions over the energy range from 1.77 eV to 3.1 eV, it was found that the absorption for $\vec{E} // \vec{c}$ is extremly suppressed. Lacking relevant theory for NbS_2 single

layers, an attempt has been made to account for observed optical anisotropy using an experimentally fitted single layer MoS_2 band model proposed by Beal et al (1972).

Single layer and single crystal anisotropy results along with a comparison with single layer and interacting layer band models will be useful in determining the effects of inter-layer interaction on the electronic structure of the layered compounds.

This thesis is only a start of the studies of the single layer systems and more fascinating properties are expected for these single layers.

BIBLIOGRAPHY

Beal, A.R., Hughes, H.P. and Liang, W.Y. 1975. J.Phys. C: Solid St. Phys., 8, 4236.

Beal, A.R., Knights, J.C. and Liang, W.Y. 1972. J.Phys. C: Solid St. Phys., 5, 3540.

Beal, A.R. and Liang, W.Y. 1973. Phil. Mag., 27, 1397.

Beal. A.R., Liang, W.Y. and Pethica, J.B. 1976. Phil. Mag., 33, 591.

Beal, A.R. and Nulsen, S. 1981. Phil. Mag., B43, 985.

Belougne, P. and Zanchetta,J.V. 1972. Ann. Univ. Abidjan, Ser. C., 8(2), 171.

Biscoe, J. and Warren, B.E. 1942. J. Appl. Phys., 13, 364.

Bozorth, R.M. and Chapin, D.M. 1942. J. Appl. Phys., 13, 320.

Brixner, L.H., 1962. J. Inorg. Nucl. Chem., 24, 257.

Bromley, R.A., Murray, R.B. and Yoffe, A.D. 1972. J. Phys. C: Solid St. Phys., 5, 759.

Consadori, F. and Frindt, R.F. 1970. Phys. Rev., B2, 4893.

Cullity, B.D., 1956. "Elements of X-ray Diffraction", Addison - Wesley.

Dash, J.G., 1982. Physics Today, 6, 15.

Di Salvo, F.J., Hull Jr, G.W., Schwartz, L.H., Voorhoeve, J.M., and Waszczak, J.V. 1973. J. Chem. Phys., 59, 1922.

Doran, N.J. and Woolley, A.M. 1981. J.Phys. C: Solid St. Phys., 14, 4257.

Fisher, W.G. and Sienko, M.J. 1980. Inorg. Chem., 19, 39.

Franklin, R.E. 1950. Acta Cryst., 3, 107.

Gamble, F.R., Di Salvo, F.J., Klemm, R.A. and Geballe, T.H. 1970. Science, N.Y., 168, 568.

Gamble, F.R., Osiecki, J.H., Cais, M., Pisharody, R., Di Salvo,F.J., and Geballe, T.H. 1971a. Science, N.Y., 174, 493.

Gamble, F.R., Osiecki, J.H., and Di Salvo, F.J. 1971b. J. Chem. Phys., 55, 3525.

Giordano, N. 1980. Phys. Rev. B22, 5635.

Hillenius, S.J. and Coleman, R.V. 1978. Phys. Rev. B18, 3790.

Jellinek, F. 1962. J. less-common Metals, 4, 9.

Jellinek, F., Brauer, G., and Muller, H. 1960. Nature, Lond. 4710, 376.

Kasowski, R.V. 1973. Phys. Rev. Lett., 30, 1175.

Klug, H.P. and Alexander, L.E. 1954. "X-ray Diffraction Procedures for Polycrystalline and Amorphous Materials", Wiley and Sons.

Liang,W.Y. 1973. J. Phys. C: Solid St. Phys., 6, 551.

Liang, W.Y. and Beal, A.R. 1976. J.Phys. C: Solid St. Phys., 9, 2823.

Maaren, M.H. and Schaefer, G.M. 1966. Phys. Letters, 20, 131.

Mattheiss, L.F. 1973. Phys. Rev., B8, 3719.

Murphy, D.W. and Hull Jr, G.W. 1975. J. Chem. Phys., 62, 173.

Parkin, S.S.P. and Beal, A.R. 1980. Phil. Mag. B42, 627.

Phillips, F.C. 1963. "An Introduction to Crystallography", Longmans.

Schäfer, H. 1962. "Chemische Transportreaktionen", Verlag Chemie Gmbh, Weinheim/Bergstrasse, Germany.
Translated by H. Frankfort. 1964. "Chemical Transport Reactions", Acad. Press, New York and London.

Scholz, G.A. and Frindt, R.F. 1980. Mat. Res. Bull., 15, 1703.

Slater, J.C. 1965. "Quantum Theory of Molecules and Solids", Vol. 2, McGraw-Hill, New York.

Straumanis, M. and Ievinš, A. 1940. "Die Präzisionsbestimmung von Gitterkonstanten Nach der Asymmetrischen Methode" Julius Springer, Berlin.

Thompson, A.H., Gamble, F.R., and Koehler Jr., R.F. 1972. Phys. Rev. B5, 2811.

Thouless, D.J. 1977. Phys. Rev. Letters, 39, 1167.

Tidman, J.P., Singh, O., Curzon, A.E., and Frindt, R.F. 1974. Phil. Mag., 30, 1191.

Wang, S. 1966. "Solid State Electronics", McGraw-Hill.

Warren, B.E. 1941. Phys. Rev., 59, 693.

Wexler, G. and Woolley, A.M. 1976. J. Phys. C: Solid St. Phys., 9, 1185.

Whittingham, M.S. 1974. J. Chem. Soc. Chem Comm.,328.

Wilson, J.A. and Yoffe, A.D. 1969. Adv. Phys., 18, 193.

Yoffe, A.D. 1974. Proc. 12th Int. Conf. on Physics of Semiconductors, ed. M.Pilkuhn (Stuttgart: Teubner).